Biomacromolecules

JANUARY 2024 VOLUME 25, NUMBER 1 pubs.acs.org/Biomac

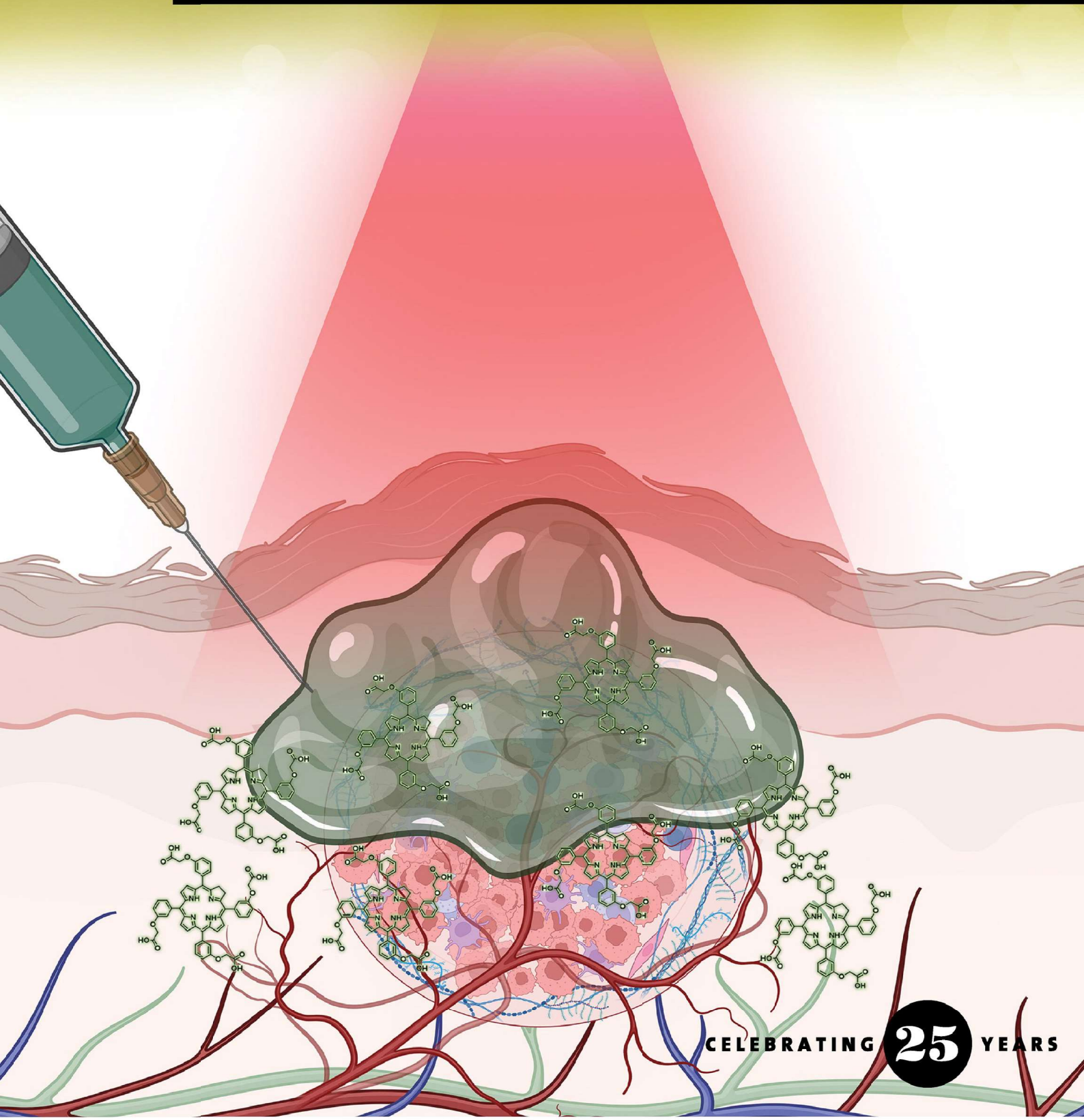

CELEBRATING 25 YEARS

ACS Publications
Most Trusted. Most Cited. Most Read.

www.acs.org

Biomacromolecules

pubs.acs.org/Biomac

Article

Antitumor Immunity Mediated by Photodynamic Therapy Using Injectable Chitosan Hydrogels for Intratumoral and Sustained Drug Delivery

Piotr Gierlich, Claire Donohoe, Kevin Behan, Daniel J. Kelly, Mathias O. Senge,* and Lígia C. Gomes-da-Silva*

Cite This: *Biomacromolecules* 2024, 25, 24−42

Read Online

ACCESS | Metrics & More | Article Recommendations | Supporting Information

ABSTRACT: Photodynamic therapy (PDT) is an anticancer therapy with proven efficacy; however, its application is often limited by prolonged skin photosensitivity and solubility issues associated with the phototherapeutic agents. Injectable hydrogels which can effectively provide intratumoral delivery of photosensitizers with sustained release are attracting increased interest for photodynamic cancer therapies. However, most of the hydrogels for PDT applications are based on systems with high complexity, and often, preclinical validation is not provided. Herein, we provide a simple and reliable pH-sensitive hydrogel formulation that presents appropriate rheological properties for intratumoral injection. For this, **Temoporfin** (***m*-THPC**), which is one of the most potent clinical photosensitizers, was chemically modified to introduce functional groups that act as cross-linkers in the formation of chitosan-based hydrogels. The introduction of −COOH groups resulted in a water-soluble derivative, named **PS2**, that was the most promising candidate. Although **PS2** was not internalized by the target cells, its extracellular activation caused effective damage to the cancer cells, which was likely mediated by lipid peroxidation. The injection of the hydrogel containing **PS2** in the tumors was monitored by high-frequency ultrasounds and *in vivo* fluorescence imaging which confirmed the sustained release of **PS2** for at least 72 h. Following local administration, light exposure was conducted one (single irradiation protocol) or three (multiple irradiation protocols) times. The latter delivered the best therapeutic outcomes, which included complete tumor regression and systemic anticancer immune responses. Immunological memory was induced as ∼75% of the mice cured with our strategy rejected a second rechallenge with live cancer cells. Additionally, the failure of PDT to treat immunocompromised mice bearing tumors reinforces the relevance of the host immune system. Finally, our strategy promotes anticancer immune responses that lead to the abscopal protection against distant metastases.

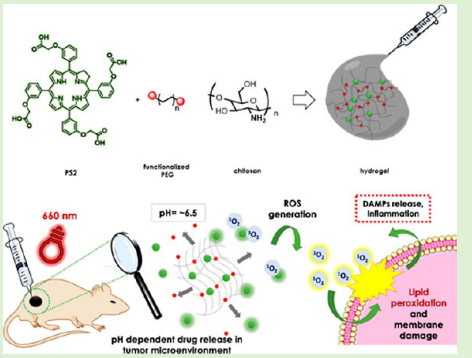

INTRODUCTION

Photodynamic therapy (PDT) has been in clinical practice for the treatment of cancer for nearly three decades. It is a combination product of a drug (named photosensitizer, PS) and a light source of a certain wavelength. Typically, the PS is administered intravenously and after a certain time interval (defined as drug-to-light interval, DLI), a laser or a light-emitting diode (LED) is used to deliver light to the tumor which, in the presence of molecular oxygen, results in the production of reactive oxygen species (ROS).[1] The oxidative stress triggered locally at the tumor induces cell death by a combination of different modalities that may lead to systemic antitumor immunity.[2]

5,10,15,20-Tetrakis(*m*-hydroxyphenyl) chlorin (*m*-THPC), with the international nonproprietary name (INN) **Temoporfin**, is one of the most potent PSs used in the clinic, with low PS doses (0.15 mg/kg) combined with a low light dose of 10 J/cm.[3] PDT using ***m*-THPC** combines efficient cell killing with the activation of anticancer immune responses, which are highly dependent on the action of neutrophils. The involvement of neutrophils has been confirmed by several studies which demonstrated that neutrophil inhibition significantly compromises the effectiveness of ***m*-THPC**-based PDT.[4−6]

Owing to the poor water-solubility of ***m*-THPC** (Log $P_{oc/w}$ ∼ 9.24), it is employed in clinical applications as a formulation based on a mixture of anhydrous ethanol and propylene glycol. This formulation is marketed under the trade name **Foscan**.[7,8] To avoid precipitation, **Foscan** administration requires a slow intravenous infusion through an indwelling catheter, which causes patient's discomfort. The high hydrophobicity of ***m*-THPC** impacts its pharmacokinetics and biodistribution. While precipitation might occur in the blood compartment after

Received: July 13, 2023
Revised: September 19, 2023
Published: October 27, 2023

Downloaded via UNIVERSIDADE DE COIMBRA 00500 on January 10, 2024 at 13:47:53 (UTC).
See https://pubs.acs.org/sharingguidelines for options on how to legitimately share published articles.

ACS Publications

© 2023 The Authors. Published by American Chemical Society

administration, disaggregation occurs upon its interaction with the blood lipoproteins and cellular membranes, which is followed by a very slow redistribution to the target cells.[9] For this reason, a DLI of 4 days is required clinically for optimal results with **Foscan**.[10] Its high lipophilicity also compromises an efficient penetration across the tumor mass which could increase the likelihood of tumor recurrence.[9,11,12] Additionally, the slow clearance of ***m*-THPC** contributes to unspecific accumulation in the skin, which is associated with weeks to months of skin and eye photosensitivity. This results in the necessity for periods without sunlight exposure, thus interfering with the patients quality of life.[13]

Strategies to deliver ***m*-THPC** specifically to the target tumor and in a controlled fashion are therefore highly desirable to overcome the issues mentioned above. An attractive strategy relies on the administration of anticancer drugs directly to the tumor and surrounding tissues. By avoiding the systemic circulation, potential benefits include enhanced bioavailability and, as a result, improved anticancer effects with reduced side effects (*e.g.*, skin photosensitivity). The accomplishment of such a goal is dependent on the development of local drug delivery strategies that permit controlled and sustained drug release while avoiding solubility issues. Prolonged release is required to ensure adequate diffusion of the PS across the tumor mass and more importantly, to permit multiple sessions of irradiations after a single administration of the PS.[14,15]

Different controlled release drug delivery systems for intratumoral administration of anticancer drugs have been the subject of various studies. Hydrogels, high-water content 3D structures prepared with cross-linked polymers, are a particularly suitable candidate for local drug delivery, and their use in PDT has attracted attention in recent years.[16,17] However, most of these studies lack preclinical validation.[18] Hydrogel delivery systems offer the advantage of enabling spatiotemporal controlled release by incorporating elements responsive to external stimulus (*e.g.*, light) or to intrinsic properties of the tumor microenvironment (*e.g.*, acidic pH).[19] The use of these activatable hydrogel-based platforms is often intended for one single local administration followed by sustained released of the drug which, in the case of PDT, may permit repeated irradiations.[15,20] The manufacture of hydrogels relies on polymers, either natural or synthetic. However, natural polymers, such as chitin and its derivative, chitosan (CS), are often preferred. CS is being widely used for different biomedical applications due to its excellent biocompatibility, low toxicity, and biodegradability.[21] It holds multiple aliphatic amine and hydroxyl groups, which are appropriate synthetic handles for the chemical cross-linking required for polymer assembly into a 3D hydrogel structure. In addition, drug payloads can be covalently bonded to CS *via* Schiff-base or *N*-acylation reactions, which also enable solubility issues to be overcome and can result in enhanced fluorescence lifetimes of PSs.[22] Based on the rate of the chemical or physical cleavage of the CS−drug bond, controlled drug delivery may be tuneable by external or internal stimuli.[23,24] For instance, protonation of the amine groups in the CS backbone can occur in an acidic tumor environment. This leads to the gradual disaggregation of the hydrogel structure and, consequently, sustained drug release.[25]

In this work, we developed a novel injectable CS-based hydrogel for the intratumoral delivery of tetrafunctionalized ***m*-THPC** derivatives, **PS1**, **2**, and **3**, that have been previously described.[26] CS-based hydrogels were formed via amide and/or imine bonds between the CS chains with the tetrafunctionalized ***m*-THPC** derivatives and with difunctionalized polyethylene glycol (PEG). The hydrogel formulated with **PS2** (herein designated as **PS2−PEG-CS**) demonstrated the highest potential, which can be attributed to the attachment of carboxyl groups to ***m*-THPC**. This enables **PS2** to exhibit good water solubility while maintaining the photophysical properties of ***m*-THPC**.[26] As a result, **PS2** efficiently generates $^1O_2$ under physiological conditions, thus making it a promising candidate for PDT. Additionally, the carboxyl groups serve as suitable synthetic handles for the preparation of the CS-based hydrogel.

PS2-PEG-CS exhibits excellent rheological properties, enabling intratumoral injection with homogeneous distribution of the PS. Driven by its self-healing properties, the hydrogel partially reforms at the tumor site after injection thus, adopting an implant-like functionality with sustained **PS2** delivery. This permits PDT protocols with multiple irradiation sessions that significantly increased the overall survival of at least two cancer mouse models. Notably, the optimized PDT protocol based on the **PS2**-loaded hydrogel stimulated host immune responses that elicit anticancer effects, even at distant sites of metastasis, and provided long-lasting memory.

MATERIALS AND METHODS

Materials. ***m*-THPC** was a gift from Biolitec. Chemicals used for hydrogel synthesis [*N*-hydroxysuccinimide (NHS) and 1-ethyl-3-carbodiimide (EDC) hydrochloride] were purchased from Sigma-Aldrich, while **PS1**, **PS2**, and **PS3** were prepared as reported before.[26] CS PROTASAN UP CL 214 was purchased from NovaMatrix. Difunctionalized PEG was synthesized according to the literature protocol.[27] CT26 cells (ATCC CRL-2638) and B16F10 (kindly given by IPO, Porto, Portugal) were cultured in Dulbecco's modified Eagle's medium (DMEM, Sigma-Aldrich) supplemented with 10% (v/v) heat-inactivated fetal bovine serum (Invitrogen), 100 U/mL penicillin, and 100 ng/mL streptomycin (Invitrogen). The Image-iT lipid peroxidation kit for live cell analysis was obtained from Thermofisher. Z-VAD-FMK, ferrostatin, necrostatin-1, and BAPTA were obtained from Sigma. Animal experiments were performed in compliance with the Portuguese animal health authority, Direção-Geral da Alimentação e Veterinária authorization, under the authorization number 0421/000/000/2020. C57BL/6J (female), BALB/c (male), or BALB/c nude mice (male) were provided by Charles River Laboratories. Mice were sex- and age-matched, with most mice at 8−12 weeks of age and approximately 20−25 g of weight.

Methods. *Preparation of CS-Based Hydrogels Containing **m*-THPC** Derivatives.* CS was dissolved in phosphate-buffer saline (PBS) (30 mg/mL) and stirred for 24 h to completely dissolve the polymer. Activation of the carboxylic acid moieties of **PS2** (0.765 mg) was achieved by an initial incubation with NHS (0.5 mg) and EDC hydrochloride (0.5 mg) for 30 min. Then, CS solution (0.4 mL) was mixed with 0.17 mL of each PS (**PS1**, **PS2**, and **PS3**) dissolved in DMSO (4.5 mg/mL) followed by the addition of 0.1 mL of the functionalized PEG dissolved in distilled water (12 mg/mL). Gelation occurred within 2 min upon vigorous mixing, followed by immersion in ethanol (40%), which was performed to remove unreacted materials and excess DMSO. The same procedure was used to obtain empty hydrogel (without PS) that was included as control in some experiments.

*Characterization of the Hydrogels Containing **m-THPC** Derivatives.* The viscoelastic properties of the cross-linked hydrogels were determined by rheological measurements that included amplitude sweep, frequency sweep, and recovery studies. These experiments were carried out with a modular compact MCR 301 Rheometer (Anton Paar, Graz, Austria) using parallel plates of 25 mm diameter with a measuring gap of 1.0 mm at 25 °C. The hydrogel was placed between the parallel plate, and a solvent trap was added to the platform to avoid evaporation of water. These experiments were performed in the linear viscoelastic (LVE) region of each hydrogel, which was in the range of 0.1−10 Hz.

https://doi.org/10.1021/acs.biomac.3c00591
Biomacromolecules 2024, 25, 24−42

In another set of experiments, the self-healing ability of the **PS1-PEG-CS** and **PS2-PEG-CS** hydrogels was evaluated macroscopically after the hydrogel was cut in half. Then, the two samples were placed together during 60 min at room temperature. Photographs were taken at 20 min intervals to record the hydrogel recovery into the original shape. In another approach, hydrogels were loaded into syringe and extruded through the needle into a vial, and the rehealing process was monitored macroscopically in time.

The cross-linking efficiency was determined for each batch of newly formed hydrogel. This parameter quantifies the exact amount of PS molecules that formed chemical bonds within the CS network. To determine this, three samples (∼30 mg) of each hydrogel were collected and totally disaggregated by adding 200 μL of acetic acid/PBS (1:1) solution. After a 10-fold dilution in DMSO, the absorbance of each PS was measured at 652 nm. The molar absorption coefficient of each PS was used, according to the Beer−Lambert law, to calculate the exact amount of PS in the hydrogel.

Impact of the pH on PS Release. Approximately 20 mg of each hydrogel was incubated in 2 mL of PBS at different pH (7.5, 6.5, and 5.0) at 37 °C. At the indicated time points (from 0 to 24 h), a sample of 50 μL of the release buffer was withdrawn, which was followed by 10× dilution to guarantee good PS solubilization. For each PS, a calibration curve was performed in PBS/DMSO (1:10 ratio) at concentrations ranging from 0 to 8 μM. The PS fluorescence was measured in a microplate reader (Biotek Synergy HT) using 420/40 nm excitation and 645/20 nm emission filters. A sample of each hydrogel was then totally disrupted by the addition of acetic acid/PBS (1:1) to entirely release the entrapped PS. The fluorescence of each PS after the acidic rupture of the hydrogel was assumed as 100% of release.

Aggregation Study. Aggregation studies were conducted with the three ***m*-THPC** derivatives (stock solution in the concentration range 1.04−1.1 mM). An equal volume of each PS stock solution (in DMSO) was diluted in PBS (0.4% DMSO) and in pure DMSO. Absorption spectra of each solution were recorded on a JASCO V-730 spectrophotometer. Comparison of the spectra obtained in pure DMSO with the one in 0.4% DMSO inferred the level of self-aggregation.

*Dark Toxicity and Phototoxicity of **m-THPC** and **PS1**, **PS2**, and **PS3** Derivatives.* B16F10 (6000 cells/well) or CT26 (6000 cells/well) cancer cells were seeded in 96-well plates and allowed to adapt for 24 h. Cells were then treated with ***m*-THPC** or **PS1**, **PS2**, and **PS3** derivatives in a concentration range from 2.5 to 80 μM during 24 h. After this, cells were washed with medium, and cellular viability (dark toxicity) was evaluated after 24 h.

Phototoxicity was evaluated in parallel experiments using two sets of concentrations of ***m*-THPC** and its tetrafunctionalized derivatives **PS1**, **PS2** and **PS3**: from 0.3125 to 10 μM (LD = 0.4 or 2 J/cm^2) and from 1.25 to 40 μM (LD = 4 J/cm^2). After an incubation of 24 h with each PS, cells were washed with medium, which was followed by illumination with LED at 660 nm (Wolezek). A correction factor from the overlap of the absorption spectra between the LED and each PS was calculated and applied in order to achieve accurate light doses.[28] A LD of 0.4 and 2 J/cm^2 was used for the concentration range of 0.3125 to 10 μM, whereas a LD of 4 J/cm^2 was used for the concentration range of 1.25 to 40 μM. Cellular viability was evaluated 24 h post-illumination.

Phototoxicity experiments were also conducted upon activation of the PSs in the extracellular environment. For this, ***m*-THPC** and its derivatives (2.5 to 80 μM) were added to the cells which were immediately illuminated with a LD of 4 or 15 J/cm^2. After 15 min, cells were washed, and fresh medium was added. Cellular viability was evaluated 24 h later.

The resazurin reduction assay (Alamar Blue) was used to infer cell viability. For this, cells were incubated with resazurin (0.01 mg/mL) for approximately 2 h, and the fluorescence of the metabolic product, resorufin, was measured in a microplate reader (Biotek Synergy HT) using 528/20 nm excitation and 590/35 nm emission filters. The level of resazurin metabolization by the untreated cells (control) was assumed as 100% viability.

Cellular Uptake. B16F10 melanoma cancer cells (35,000 cells/well) were seeded in 24-well plates and allowed to adapt for 24 h. Cells were then incubated with ***m*-THPC**, **PS1**, **PS2**, and **PS3** at a concentration of 8 μM during 24 h. Afterward, cells were washed twice with DMEM followed by lysis using DMSO + 1% Triton X-100. Cell lysates were centrifuged (2000 rpm, 5 min), and the supernatant (containing the internalized PS) was collected and submitted to the fluorescence measurement. To quantify the absolute amount of internalized PS, a calibration curve of each PS in lysis buffer was prepared, with concentrations ranging from 0 to 8 μM, in the lysis buffer. Fluorescence measurements were carried out with a microplate reader (Biotek Synergy HT) using 460/40 excitation and 645/40 emission filters.

Evaluation of Lipid Peroxidation Using the Image-iT Lipid Peroxidation Kit. The Image-iT lipid peroxidation kit is based on the BODIPY 581/591 which intercalates into the lipid membranes of live cells. Upon oxidation by lipid hydroperoxides, its fluorescence peak shifts from ∼590 nm (red) to ∼510 nm (green), providing a ratiometric indication of lipid peroxidation. B16F10 melanoma cancer cells (50,000 cells/well) were seeded in 24-well plates. After 24 h, cells were incubated with the BODIPY 581/591 (10 μM) for 30 min. This was followed by the addition of ***m*-THPC** and **PS2** (40 μM) to the cells which were immediately illuminated with a LD of 15 J/cm^2. As positive control, cells were treated with cumene hydroperoxide (40 μM) for 2 h with the last 30 min of incubation including the presence of 10 μM BODIPY 581/591. Images were acquired on a Carl Zeiss LSM 710 confocal microscope using a laser at 488 nm for the excitation of the BODIPY probe. Cell segmentation and signal quantification were performed using ImageJ software, and lipid peroxidation was calculated based on the ratio between 590 (reduced form) and 510 (oxidized form) signals. Additionally, the fluorescence intensity of the oxidized BODIPY probe was quantified by flow cytometry (Novocyte TM 3000 ACEA) upon excitation with the laser at 488 nm, and fluorescence collection was carried out using the filter 530/30 nm.

Mechanism of Cell Death. B16F10 cancer cells (7000 cells/well) were seeded in 96-well plates. After 24 h of incubation, inhibitors of different cell death modalities such as apoptosis (Z-VAD-FMK, 25 μM), ferroptosis (ferrostatin, 5 μM), necroptosis [Necrostatin-1 (25 μM)] or the Ca^{2+} chelator, BAPTA-AM (5 μM), were added to the cells. The inhibitors were removed, and **PS2** was added to the cells (from 2.5 to 80 μM) into the appropriate triplicate wells, followed by irradiation (LD = 15 J/cm^2). Afterward, cells were washed, and fresh medium containing each inhibitor was added. Cellular viability was evaluated 24 h later by the resazurin assay.

*Microscopic Evaluation of the Morphological Changes Induced by Photoactivated **PS2** and **m-THPC**.* B16F10 cells (70,000 cells/well) were seeded in 24-well plates at a final volume of 500 μL of DMEM. 24 h later, ***m*-THPC** (40 μM) and **PS2** (40 μM) were added. The cells were immediately irradiated with a LD of 15 J/cm^2 and then washed with PBS. Finally, Hoechst (3,24 μM) and propidium iodide (PI) (0.002 mg/mL) were added, incubated for 24 h, and observed under a fluorescence microscope (Olympus CKX41 microscope with an Olympus U-RFLT50 fluorescence system).

Scanning Electron Microscopy and Transmission Electron Microscopy. For scanning electron microscopy (SEM) imaging, the hydrogel was freeze-dried to completely remove any water from the porous structure. Subsequently, the hydrogel samples were coated with a 5 nm layer of gold under vacuum, and the imaging was performed (JSM-6610A) using a scanning electron microscope (JEOL, Tokyo, Japan). For transmission electron microscopy (TEM) imaging, **PS2-PEG-CS** hydrogel was placed on a grid and scanned to observe the porous structure of the polymer scaffold. Images were taken using a Hitachi H-800 microscope (Hitachi High-Technologies).

Ultrasound Imaging. **PS2-PEG-CS** and **PS2-PBS** distribution at the injection site was assessed using Vevo LAZR-X multimodal imaging system from Fujifilm-VisualSonics (Toronto, Canada). For the imaging procedure, animals were anesthetized with isoflurane (1.5−2.5%). Each animal was placed in the right position, and tumor regions were covered with standard gel for ultrasound. When the transducer was in a perpendicular position relative to the center of the tumor, the scanning was initialized, and injection of **PS2-PEG-CS** or **PS2-PBS** was performed. The images obtained were analyzed by using VevoLab software.

https://doi.org/10.1021/acs.biomac.3c00591
Biomacromolecules 2024, 25, 24−42

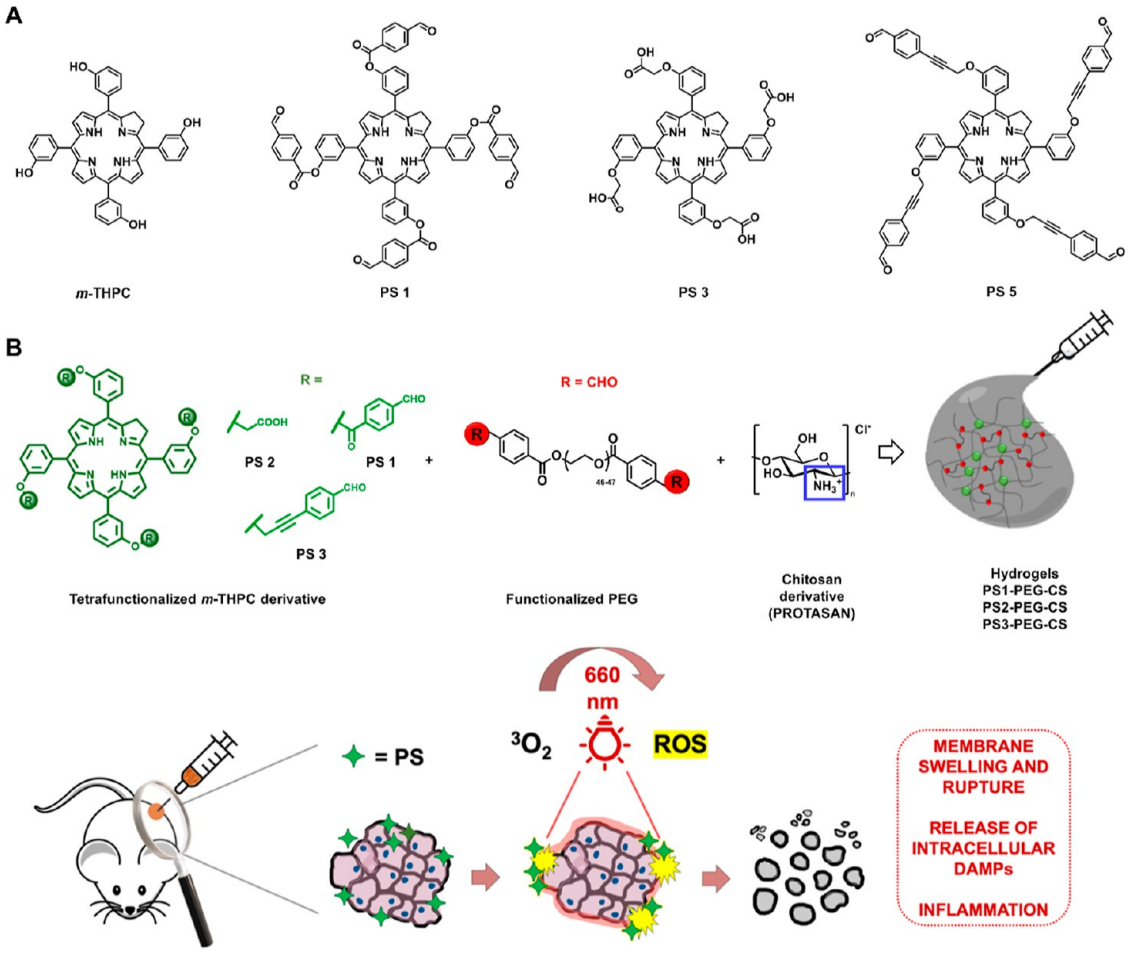

Figure 1. Schematic illustration of covalently cross-linked CS-based hydrogel photodynamic therapy against cancer. (A) Molecular structure of ***m*-THPC** and its tetrafunctionalized derivatives, **PS1**, **2**, and **3**.[26] (B) Schematic representation of the hydrogel formation process and application for PDT.

In Vivo and Ex Vivo Fluorescence Imaging. All of the animal experiments were approved by the Portuguese Animal and Food Authority (DGAV authorization 0421/000/000/2020). Tumors were established by subcutaneous injection of 350,000 CT26 cells in male Balb/c mice or 500,000 B16F10 cells in female C57BL/6 mice. Mice hair in the tumor area was removed with a commercial hair removal cream. When tumors reached *ca.* 5 mm, **PS2-PEG-CS** hydrogel or **PS2-PBS** solution (5.6% DMSO) was injected intratumorally into B16F10 or CT26 tumors. The administered **PS2** dose was 0.08 mg/mouse. Hydrogel formulation **PEG-CS**, which does not contain **PS2** in its structure, was included as a negative control. Biodistribution of **PS2** was assessed by measuring its fluorescence by means of an IVIS Lumina XR *in vivo* imaging system (Caliper LifeSciences, Hopkinton, MA, USA) with an excitation at 430 nm and an emission at 570−650 nm. Mice were kept under anesthesia with isoflurane using an XGI-8 Gas Anesthesia Delivery System (PerkinElmer, USA). Images were acquired immediately before and after the injection as well as at 3, 6, 24, 48, 72, and 168 h postinjection. All images were taken in the automatic mode and are presented in the same color scale which is independent for both tumor models. Fluorescence signals were quantified using Living Image 4.5.2 software (IVIS Imaging Systems) and were expressed as the radiant efficiency $(p/s/cm^2/sr)/(\mu W/cm^2)$. A region-of-interest (ROI) around the tumor was applied for all images and compared over time and between treatment groups. At the last time point, animals were sacrificed, and organs (bladder, kidney, muscle, liver, spleen, and tumor) were collected and placed on a Petri dish. Fluorescence images of each organ were recorded by applying the abovementioned conditions.

*PDT Using **PS2-PEG-CS** Hydrogels for the Treatment of CT26 or B16F10 Tumors.* Tumors were established by subcutaneous injection of 350,000 CT26 cells in the flank of male Balb/c mice or 500,000 B16F10 cells in the flank of female C57BL/6 mice. Mice hair in the tumor area was removed with commercial hair removal cream 4 to 6 days postinoculation. **PS2** formulation and free **PS2** were injected intratumorally when the tumor reached *ca.* 5 mm in diameter. For CT26 tumors, 0.07 mg of **PS2** was used, whereas 0.08−0.1 mg of **PS2** was required for B16F10 tumors. Tumor illumination (area 1.77 cm^2) was performed 24 h later using a LED at 660 nm (Wolzek), and a LD of 20 or 40 J/cm^2 was delivered, respectively, for CT26 or B16F10 tumors. In parallel experiments, tumors were submitted to three irradiations at 24, 48, and 72 h postintratumoral administration of the PS. Tumor growth was measured twice a week with a caliper, and the volume was calculated using the formula $V = (a \times b^2)/2$, where a corresponds to the major diameter and b to the minor diameter. The humane end point was selected as 12 mm diameter of the tumor size.

Evaluation of Antitumor Immune Memory Mediated by PS2-PEG-CS-Based PDT. Male Balb/c mice that remain tumor free 60 days post **PS2-PEG-CS**-based PDT were considered cured. At this point, these mice were rechallenged with a subcutaneous inoculation of 350,000 CT26 cells, or with 350,000 4T1 cells, in the contralateral untreated flank. Age-matched group of naïve Balb/c mice were used as negative control for both CT26 and 4T1 tumor growth. Tumor growth was followed as mentioned above.

*Efficacy of **PS2-PEG-CS**-Based PDT in BALB/c Nude Immunocompromised Mice.* Male Balb/c nude and WT Balb/c mice were inoculated *via* subcutaneous injection of 350,000 CT26 cancer cells in the right flank. **PS2-PEG-CS** hydrogel (0.04 mg) was injected

https://doi.org/10.1021/acs.biomac.3c00591
Biomacromolecules 2024, 25, 24−42

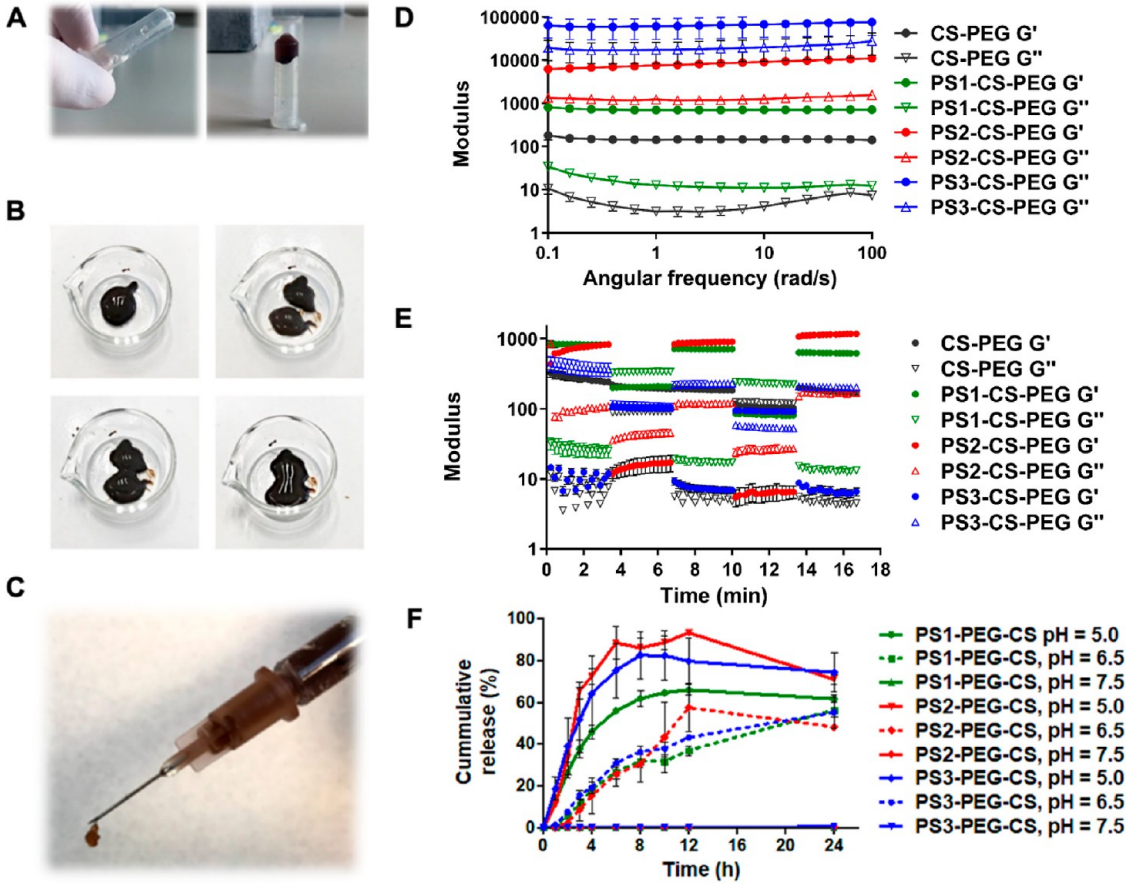

Figure 2. Preparation and characterization of CS-based hydrogels containing ***m*-THPC** derivatives. (A) From viscous solution of CS (right) to cross-linked hydrogel loading **PS2**; (B) macroscopical evaluation of the self-healing properties of the **PS1-PEG-CS** hydrogel during 1 h after its physical disruption; (C) injectable properties of the **PS2-PEG-CS** hydrogel; (D) storage (G') and loss (G') moduli of the hydrogel formulations containing **PS1**, **2**, **or 3** as a function of angular frequency at a fixed strain of 5% ($n = 3$); (E) self-healing properties of all hydrogel formulations demonstrated by continuous step strain measurements (5% strain → 300% strain → 5% strain → 600% strain → 5% strain) ($n = 3$); and (F) pH-dependent release of **PS1**, **2**, and **3** from their hydrogel scaffold at pH of 5.0, 6.5, and 7.5 ($n = 2$).

intratumorally when the tumors reached *ca.* 5 mm in diameter. After 24, 48, and 72 h, tumor irradiation was performed, and a LD = 20 J/cm^2 was delivered at each time. Tumor growth was followed as mentioned above.

*Abscopal Effects of PDT with **PS2-PEG-CS** on Distant and Untreated Metastases.* Male Balb/c mice were inoculated *via* subcutaneous injection of 350,000 CT26 cancer cells in the right flank followed by a second inoculation 10 days later on the contralateral flank. On the same day, intratumoral injection of the **PS2-PEG-CS** hydrogel or **PS2-PBS** solution (0.04 mg **PS2**/mouse) was performed in the primary tumor. After 24, 48, and 72 h, tumor irradiation was performed, and a LD = 20 J/cm^2 was delivered at each time. Tumor growth of the primary and secondary tumors was followed until the animals reached the humane end point.

Statistical Analysis. The results from *in vitro* studies are presented as the mean ± standard error (SEM) of 2−3 independent experiments, each one in triplicates. One-way ANOVA with Dunnett's post-test or two-way ANOVA with the Bonferroni post-test was used to determine statistically significant differences of the means between the indicated groups. Survival analysis of mice was performed by means of a Kaplan−Meier estimator with the long-rank (Mantel-Cox) test to evaluate the significance of the differences between different PDT-treated groups. Statistical differences were presented at probability levels of $p < 0.05$ *, $p < 0.01$ **, and $p < 0.001$ ***.

RESULTS AND DISCUSSION

Synthesis and Characterization of CS-Based Hydrogels Containing *m*-THPC Derivatives. CS-based hydrogel formulations were prepared by taking advantage of the tetrafunctionalized derivatives (**PS1**, **2**, and **3**) previously synthesized and characterized (Figure 1A).[26] The developed hydrogels were composed of CS, difunctionalized PEG, and one of the ***m*-THPC** derivatives. Chemical structures of PEG and CS and characterization of the difunctionalized PEG are presented in Figure S1. **PS1-PEG-CS** and **PS3-PEG-CS** hydrogels were prepared using a one-pot reaction by directly mixing CS with **PS1**, or **PS3**, and the difunctionalized PEG (Figure 1B). The latter is critical to obtain cross-linked hydrogels with imine bonds.[29] In contrast, conjugation of **PS2** to CS required an initial step of activation of the carboxylic acid groups which was achieved by the addition of NHS and EDC hydrochloride. The obtained intermediate product, O-acylisourea, enabled further reactions with the amine groups.[30] Activated **PS2** was subsequently added to CS, which was followed by the addition of PEG to yield the **PS2-PEG-CS** hydrogel. For the three ***m*-THPC** derivatives, gelation of **PS1-PEG-CS**, **PS2-PEG-CS**, and **PS3-PEG-CS** was observed within 2 min (Figure 2A).

The obtained hydrogels were characterized by using FT-IR spectroscopy. The IR spectra of **PS1-PEG-CS** and **PS3-PEG-CS** display a peak between 1650 and 1600 cm^{-1} which is absent for CS or PEG alone (Figure S2). This peak is attributed to an imine bond (C═N) between CS and the PS.[31] IR spectra of **PS2-PEG-CS** confirm the cross-link *via* amide bonds as new

https://doi.org/10.1021/acs.biomac.3c00591
Biomacromolecules 2024, 25, 24−42

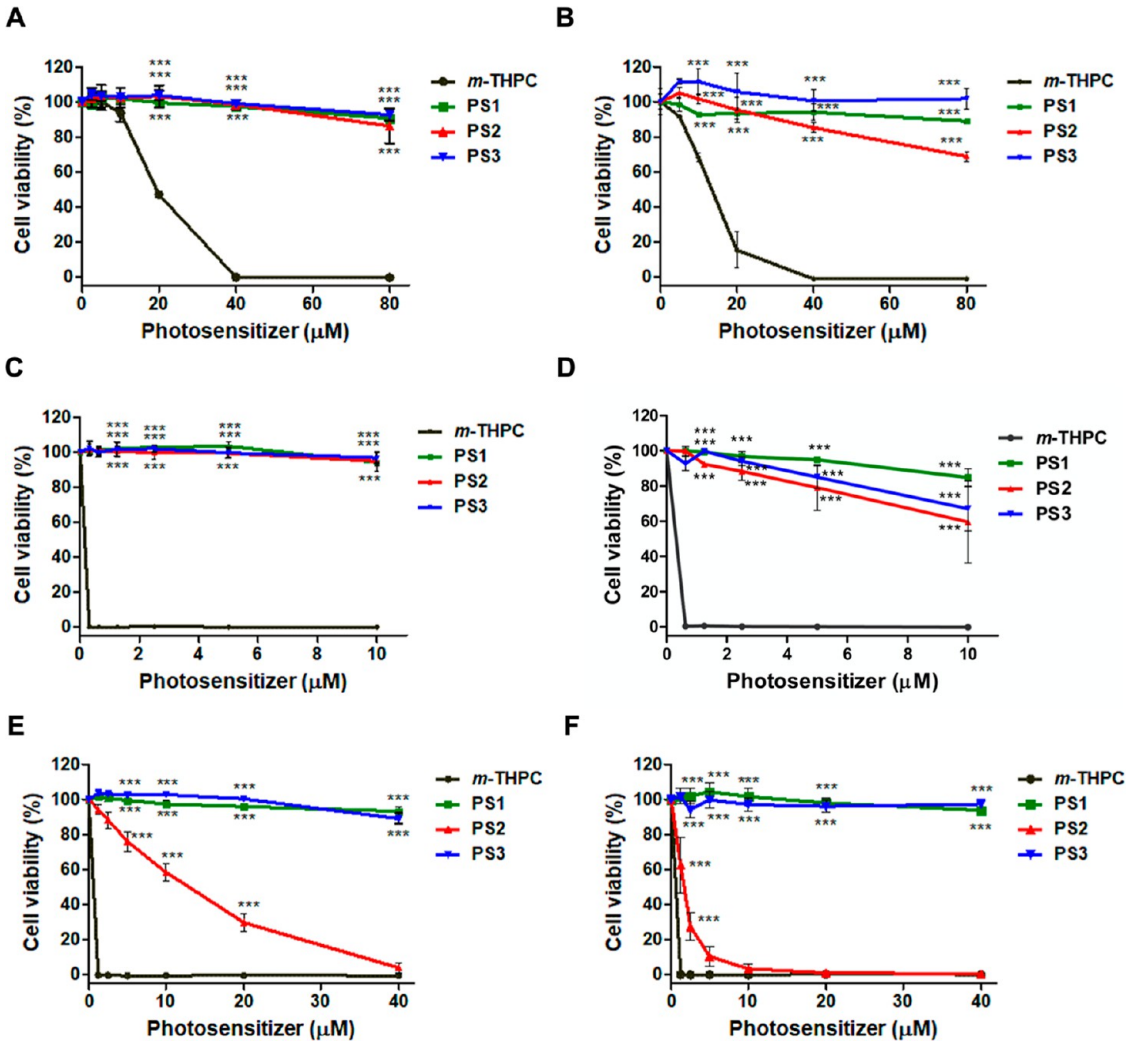

Figure 3. Dark toxicity and phototoxicity of ***m*-THPC** and the tetrafunctionalized derivatives **PS1**, **2**, and **3**. Dark toxicity evaluated in (A) B16F10 and (B) CT26 cancer cells; (C) phototoxicity of ***m*-THPC** and tetrafunctionalized derivatives **PS1**, **2**, and **3** incubated with B16F10 melanoma cells for 24 h followed by illumination at 660 nm with a LD of 0.4 J/cm^2; (D) phototoxicity of ***m*-THPC** and tetrafunctionalized derivatives **PS1**, **2**, and **3** incubated with B16F10 melanoma cells for 24 h followed by illumination at 660 nm with a LD of 2 J/cm^2; and (E) phototoxicity of ***m*-THPC** and tetrafunctionalized derivatives **PS1**, **2**, and **3** incubated with B16F10 melanoma cells or (F) with CT26 colon carcinoma cells for 24 h followed by illumination at 660 nm with a LD of 4 J/cm^2; ***$p < 0.001$ *vs* ***m*-THPC**.

absorption bands between 3200 and 3600 and 1650−1700 cm^{-1} were observed (Figure S3).[32] The aldehyde group of the functionalized PEG was absent in all of the hydrogel formulations, which suggested cross-linking of PEG within the network (Figures S2 and S3).

The cross-linking efficiency has a significant impact on several features of the hydrogel including the viscoelastic properties, drug loading, and release efficiency.[33] Therefore, the exact amount of **PS1**, **2**, or **3** was quantified in three samples of each CS-based hydrogel to establish the average amount of the PS per batch. For this, the hydrogel structure was disrupted *via* hydrolysis under acidic conditions, and the accurate concentration of the PS was determined spectroscopically using the PS molar absorption coefficient and considering the Lambert−Beer law.[34] The cross-linking efficiency in the range of 70−80% was obtained for the three ***m*-THPC** derivatives: 80.15 ± 5.73% (**PS1-PEG-CS**), 70.00 ± 7.32% (**PS2-PEG-CS**), and 79.95 ± 4.27% (**PS3-PEG-CS**). Additionally, different samples of the same hydrogel batch exhibit similar amounts of the PS (variation did not exceed 10%) indicating that the PS was homogeneously distributed within the hydrogel network.

The viscoelastic properties of the CS-based hydrogels were studied macroscopically and by rheological measurements. First, the self-healing ability of the hydrogel formulations was evaluated by cutting the hydrogel into two pieces. These reintegrated into a single mass within 1 h (Figure 2B). Next, hydrogels were loaded into a syringe barrel and extruded through a 29G needle. During extrusion, the hydrogel structure deforms, thus, enabling injection (Figure 2C). These results demonstrated that the CS-based hydrogel formulations containing ***m*-THPC** derivatives possess self-healing abilities and presented potential as injectable formulations.

Rheological measurements included amplitude and frequency sweeps as well as a recovery study. Amplitude sweep was performed to determine the LVE region, which was further used to measure the viscoelastic characteristics of the formulation (Figure S4). Next, frequency sweep measurements were preformed to evaluate and compare the viscoelastic properties of hydrogels, which are defined by storage (G') and loss (G'')

https://doi.org/10.1021/acs.biomac.3c00591
Biomacromolecules 2024, 25, 24−42

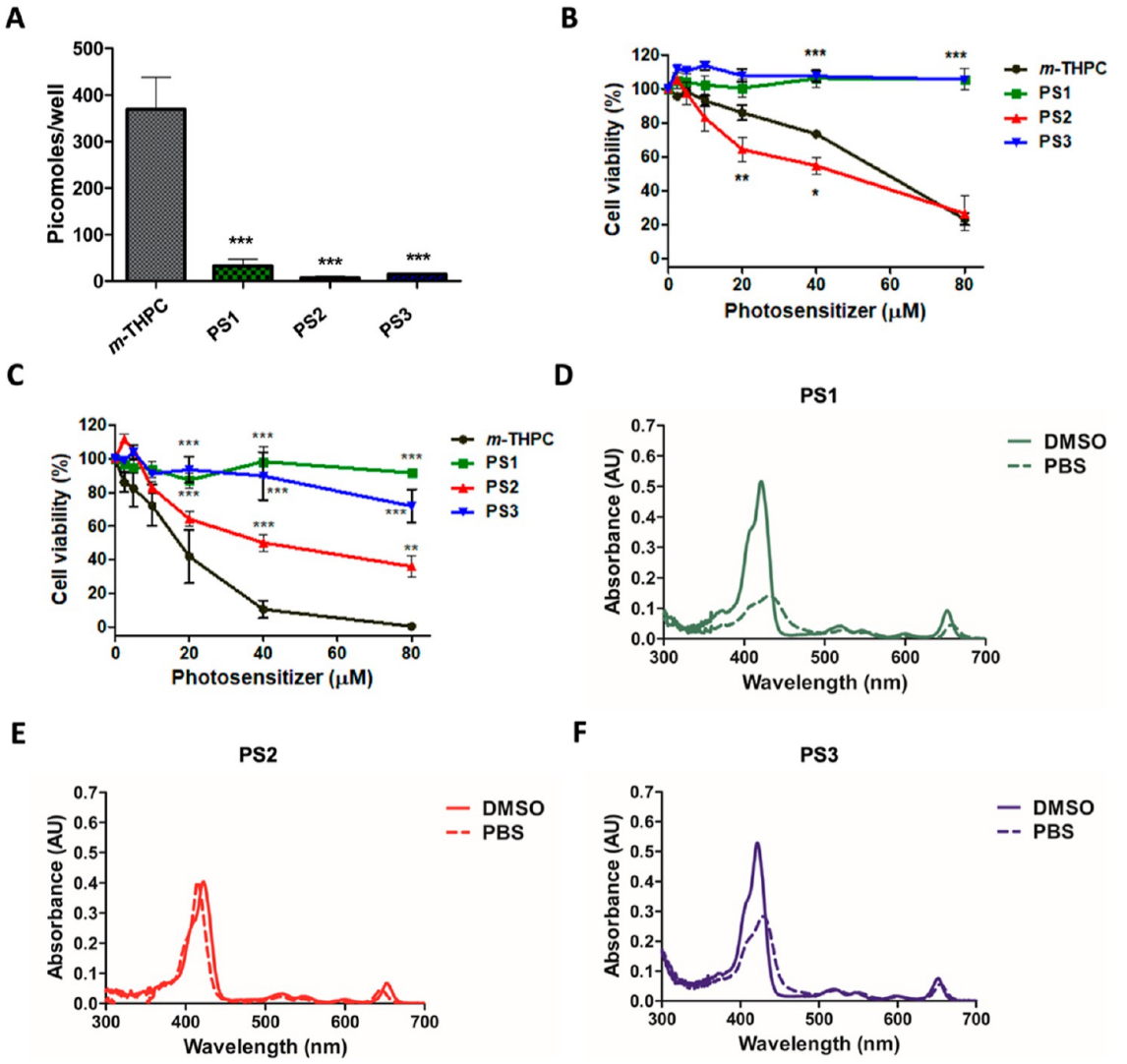

Figure 4. Cellular uptake, phototoxicity, and self-aggregation in aqueous medium of ***m*-THPC** and the tetrafunctionalized derivatives **PS1**, **2**, **and 3**. (A) Cell uptake of ***m*-THPC** and derivatives **PS1**, **2**, and **3**, after 24 h of incubation with B16F10 cancer cells. Bars indicate the mean ± SEM of three independent experiments; *** *vs* ***m*-THPC**. (B) Phototoxicity of ***m*-THPC** and tetrafunctionalized derivatives **PS1**, **2**, and **3** in B16F10 melanoma or (C) in CT26 colon carcinoma cells by using an extracellular PDT protocol with a LD of 15 J/cm^2. Each point indicates the mean ± SEM of three independent experiments; ***$p < 0.001$, **$p < 0.01$, and *$p < 0.05$ *vs* ***m*-THPC**. (D−F) Representative absorption spectra of **PS1**, **PS2**, and **PS3** recorded in pure DMSO and in PBS (0.4% DMSO).

moduli.[35] The storage modulus of the CS-based hydrogels was higher than the loss modulus, which confirmed the formation of a 3D hydrogel network. Moreover, the higher values of G' (∼1000 and more) and G'' (>10) for all hydrogels containing PS in comparison to the blank formulation (∼100 for the G' and lower than 10 for the G'') indicate that the PS increases the rigidity of the hydrogel (Figure 2D). Finally, the self-healing properties of the hydrogel networks were studied by applying strain (5, 300, and 600%) at defined time intervals.[36] The hydrogel formulations were stable at a strain of 5% but not at strain values of 300 or 600%, where the internal structure is destroyed. Of note, storage and loss moduli values of the CS-based hydrogels recovered to the original values after removal of the applied strain (Figure 2E), which confirmed their injectability.

Cross-linked hydrogels based on imine and amide bonds are expected to have pH-responsive behavior. At acidic pH, protonation of the imine and amide bonds is anticipated to trigger the release of the formulated PS in a sustained manner.[37] The PS release from the developed CS-based hydrogels was then evaluated at varied pH values (5.0, 6.5, and 7.4), at 37 °C. Our results demonstrated an accelerated drug release from the hydrogel scaffolds incubated at pH = 5 with ∼80% of PS released within 6−8 h. A slower release was observed at pH = 6.5 with only ∼50% of release after 10 h. In contrast, at pH = 7.5, no PS release was observed even 24 h after incubation (Figure 2F). These results confirm the excellent stability of the developed PS containing hydrogels at the physiological pH while showing their ability to trigger drug release in acid environments.[38] Upon release in the acidic tumor microenvironment, the PS is expected to interact with the cancer cells to exert its biological action. The phototoxicity of the free PSs was then evaluated *in vitro* in two cancer cell lines.

Phototoxicity and Uptake of *m*-THPC Tetrafunctionalized Derivatives: PS1, 2, and 3. Studies conducted in CT26 and B16F10 cells in the absence of light indicate that the tetrafunctionalized ***m*-THPC** derivatives, **PS1**, **2**, and **3**, were not cytotoxic at concentrations up to 80 μM (Figure 3A,B). In

https://doi.org/10.1021/acs.biomac.3c00591
Biomacromolecules 2024, 25, 24−42

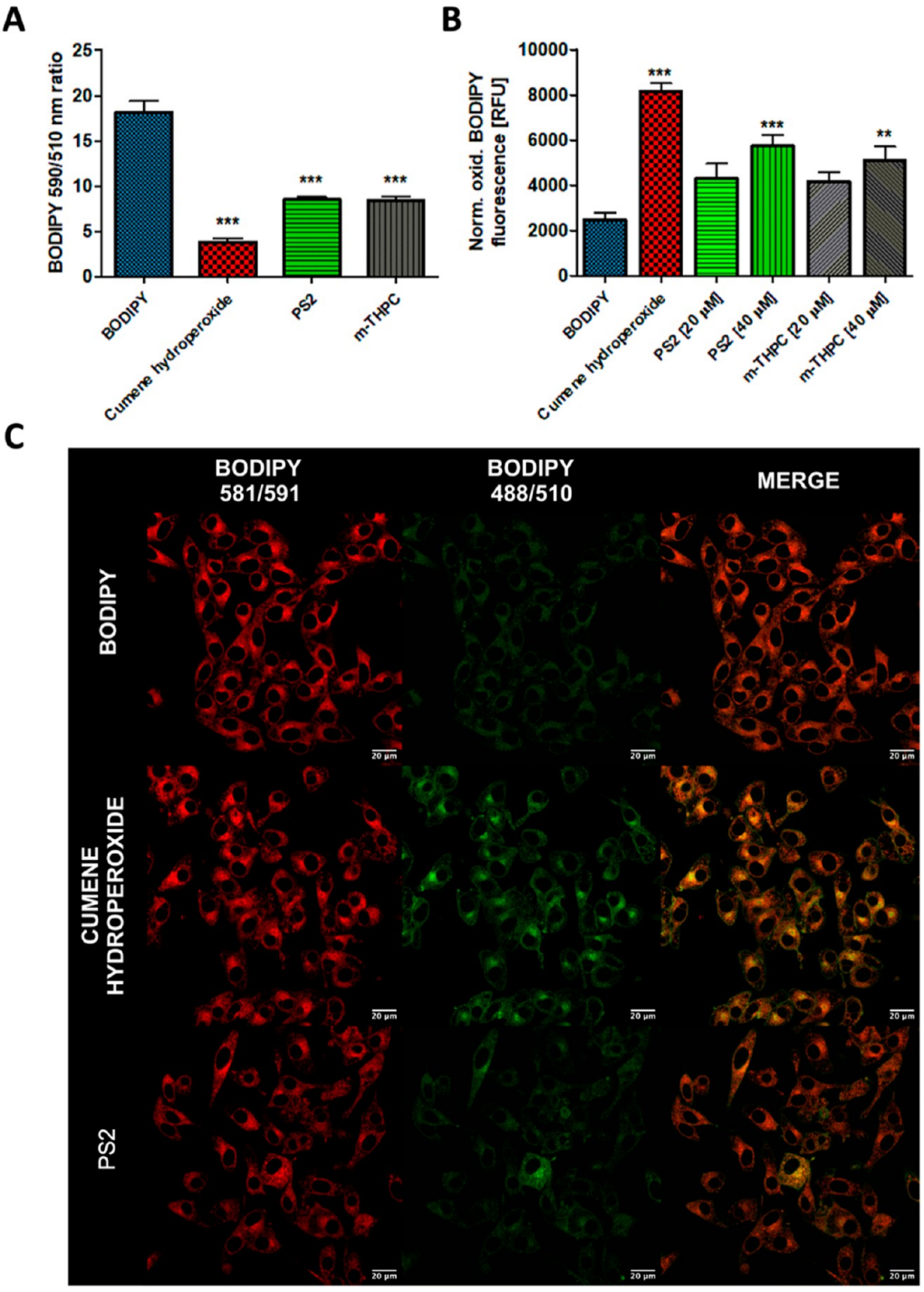

Figure 5. ***m*-THPC** and **PS2** activated extracellularly induced significant lipid peroxidation. (A) Quantitative analysis of lipid peroxidation, obtained by the 590/510 fluorescence ratio, on B16F10 cancer cells after extracellular PDT with **PS2** (40 μM). Bars indicate the mean ± SEM of triplicates from one representative experiment with B16F10 cells, ***$p < 0.001$ *vs* untreated cells incubated with the BODIPY. (B) Oxidation of the BODIPY 581/591 C11 was evaluated by flow cytometry in B16F10 cancer cells after extracellular PDT with **PS2** (20 and 40 μM) and ***m*-THPC** (20 and 40 μM). Cumene hydroperoxide (40 μM) was included as positive control. Results are expressed as the mean ± SEM of three independent experiments, ***$p < 0.001$ and **$p < 0.01$ *vs* untreated cells incubated with the BODIPY. (C) Representative images of lipid peroxidation on B16F10 cancer cells caused by photoactivated **PS2** (40 μM). Reduced (red) and oxidized (green) forms of the BODIPY 581/591 probe were obtained via confocal microscopy; scale bar = 20 μm; cumene hydroperoxide (10 μM) was used as a positive control.

contrast, ***m*-THPC** displayed significant dark toxicity when concentration exceeded 20 μM, with IC_{50} values of 19.39 and 11.19 μM for B16F10 and CT26 cells, respectively.

Unexpectedly, ***m*-THPC** derivatives (from 0.3125 to 10 μM) were not phototoxic when a LD (light dose) of 0.4 or 2 J/cm^2 was delivered. This was in sharp contrast with ***m*-THPC**, which killed 100% of B16F10 cells at all the tested conditions (Figure 3C,D). By augmentation of the PS concentration and the LD, the cell viability decreased with the photoactivated **PS2** derivative. The former mediates over 90% cell death when

https://doi.org/10.1021/acs.biomac.3c00591
Biomacromolecules 2024, 25, 24−42

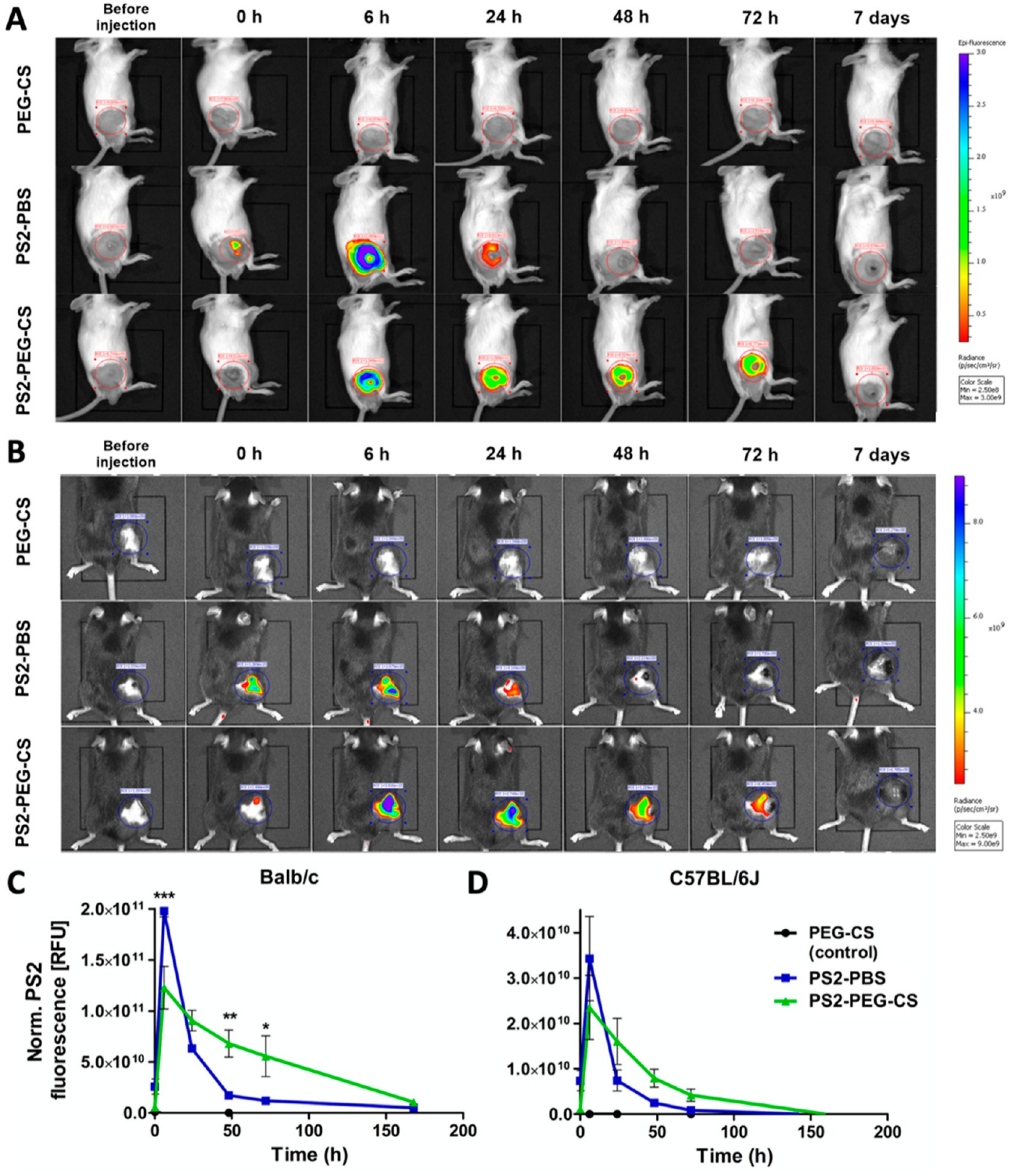

Figure 6. Time-dependent *in vivo* fluorescence images of **PS2-PEG-CS** and free **PS2**. (A) Indicated formulations (0.08 mg **PS2**/mouse) were directly injected in CT26 tumors (Balb/c mice) or in (B) B16F10 tumors (C57BL/6J mice). At various time points, *in vivo* fluorescence images of the whole body were taken. Each group contained three mice with the exception of the control group that only included one animal. (C,D) Quantitative analysis of the obtained fluorescence images. The background signal detected before **PS2** injection was subtracted from each signal obtained at varied time points. Each point represents the mean ± SEM of three mice; ***$p < 0.001$, **$p < 0.01$, and *$p < 0.05$ **PS2-PBS** *vs* **PS2-PEG-CS**.

used at 40 μM with a DL of 4 J/cm^2. However, **PS1** and **3** did not exhibit any phototoxicity (Figure 3E). The same trend of activity was observed in CT26 cells but with a higher sensitivity to the PDT treatments. For example, cell viability was observed as lower than 20% for concentrations higher than 2.5 μM (LD = 4 J/cm^2) (Figure 3F). This was reflected in the **PS2** IC_{50} that is 20 times lower for CT26 (0.88 μM) cells than that for B16F10 cells (19.99 μM). The poor phototoxicity of **PS1**, **2**, and **3** derivatives was unexpected considering that the photophysical properties of these molecules are similar to the ones of the ***m*-THPC**

https://doi.org/10.1021/acs.biomac.3c00591
Biomacromolecules 2024, 25, 24−42

counterpart.[26] Intrigued by these discrepancies, we next investigated the cell internalization of ***m*-THPC** derivatives by exploiting their inherent fluorescence.

Uptake of **PS1**, **2**, and **3** derivatives was ∼10-fold lower than ***m*-THPC** cell uptake (Figure 4A). The impaired uptake of the ***m*-THPC** derivatives might be explained by the chemical modifications that were introduced on ***m*-THPC**. These modifications significantly increased the molecular weight and introduced changes to the polarity and amphiphilicity of the ***m*-THPC** derivatives, which impair their ability to diffuse across the cell membranes and therefore, reduced activity.[39,40] However, a few studies have shown that singlet oxygen ($^1O_2$) produced extracellularly (in the cell culture medium) can induce cell death.[41,42] Thus, the phototoxicity of the ***m*-THPC** derivatives was evaluated by using an extracellular PDT protocol in which cells were irradiated (LD = 15 J/cm^2) immediately after the addition of the PS. Significant reduction of the cellular viability was observed when ***m*-THPC** or **PS2** were photoactivated extracellularly. **PS1** and **PS3** counterparts (Figure 4B,C), in contrast, did not present significant effects. The superiority of ***m*-THPC** might be explained by its higher amphiphilicity and, therefore, greater propensity to interact with the lipid bilayer.[43,44] However, it was less clear what was mediating the higher efficacy of **PS2** when compared with that of the other derivatives.

Aggregation of a PS in aqueous media reduces $^1O_2$ and fluorescence quantum yields, shorts triplet state lifetime, and lowers absorbance, which ultimately impairs the PS efficacy.[45] The absorbance of **PS1** and **PS3** in PBS containing 0.4% DMSO was significantly decreased, and the absorption bands were broadened (two-fold decrease of the Soret band) compared to the spectra of these molecules in pure DMSO. This suggests self-aggregation.[46,47] In contrast, the **PS2** spectra was identical in both PBS and pure DMSO. The differences on **PS1**, **2**, and **3** spectra can be attributed to their different polarities. **PS2** is a water-soluble molecule, while **PS1** and **PS3** display hydrophobic properties (Figure 4D−F). Then, it is expected that $^1O_2$ generating efficiencies of **PS1** and **PS3** is significantly impaired in aqueous media, thus explaining their lack of activity.

Mechanism of Cell Death Mediated by PDT with PS2 Activated Extracellularly. Next, we investigated the **PS2** mode of cell killing. $^1O_2$ produced extracellularly has been shown to trigger accidental necrosis, likely through its action on the cell membrane. This has been shown with PSs which lack the ability to cross the cell membrane and with PSs that accumulated at the cellular membrane.[42,48] Images obtained by light transmission and fluorescence microscopy suggested that photoactivated **PS2** kill cells mainly by accidental necrosis. The control group exhibited the characteristic morphology of melanoma cells with the shape of spindle- and epithelial-like cells and with a homogeneous Hoechst distribution on the cell nuclei (Figures S5 and S6). A negligible signal for PI was observed confirming that the population of cells does not exhibit signs of death. In contrast, cells adopted a round shape after PDT with ***m*-THPC** or **PS2** activated extracellularly (Figures S5 and S6). PDT-treated cells did not exhibit significant changes on Hoechst staining (as typically observed in apoptosis) but a strong fluorescence signal for PI was observed, which is suggestive of accidental necrosis (Figures S5 and S6).[49] This is supported by the observation that pharmacological inhibitors of different regulated mechanism (such as apoptosis, necroptosis, or ferroptosis) failed to rescue cell viability (Figure S7). Overall, accidental necrosis is suggested as the main mechanism of cell death of ***m*-THPC**, or **PS2** activated extracellularly.

Membrane damage with extensive lipid peroxidation is expected to occur for PSs activated extracellularly.[50,51] For this reason, lipid peroxidation was evaluated by means of the BODIPY 581/591 C11 (log $P_{oc/w}$ ∼ 2.5), a fatty acid analogue that accumulates at the lipid membranes (cell membrane and membrane-bound organelles). Its fluorescent shifts from 590 nm (red) to 580 nm (green) upon oxidation.[52] Confocal microscopic evaluation showed that **PS2** and ***m*-THPC** activated extracellularly induced lipid peroxidation throughout the cells. This may reflect not only the action of $^1O_2$ at the cell membrane but also the ability of lipid hydroperoxides to initiate chain peroxidation cascades which propagate oxidative stress.[53] Lipid peroxidation was quantified through the red/green fluorescence ratio, which lowers when oxidation levels increase (Figure 5A,C). These observations were confirmed by flow cytometry analysis of the oxidized form (green), which also shows that lipid peroxidation was concentration dependent (Figures 5B and S8).

Pharmacokinetics and Biodistribution of PS2-PEG-CS Hydrogel. The data obtained indicated that **PS2** has the greatest potential as a PS candidate. SEM and TEM were then used to assess the surface and internal morphologies of the CS-based hydrogel containing **PS2**. SEM images revealed that the **PS2-PEG-CS** hydrogel is a homogeneous connected structure without any agglomerates or crystalline structures on the surface (Figure S9A,B). TEM images of the hydrogel exhibited a spongelike structure with pores primarily present in the thinner sides of the hydrogel sample. The average pore size in that region ranged from 100 to 200 nm in diameter, which correlates with the good swelling properties of the **PS2-PEG-CS** hydrogel (Figure S9C,D).

Next, the **PS2-PEG-CS** hydrogel was submitted to preclinical evaluation in two subcutaneous tumor models: Balb/c mice bearing CT26 tumors and C57BL/6J mice bearing B16F10 tumors. The intratumoral administration of the hydrogel was monitored in real-time with high-frequency ultrasounds. The images showed that the hydrogel presents the advantage of more precise delivery of the PS at the treated site, while the solution of **PS2-PBS** tends to distribute to the surrounding tissues (Figure S10).

The release/retention profile of **PS2** from the CS-based hydrogel after intratumoral administration was obtained by *in vivo* fluorescence imaging. Slow and prolonged **PS2** release was observed at the tumor site, at least for 3 days, when the **PS2-PEG-CS** hydrogel scaffold was used (Figure 6A,B). Directly after **PS2-PEG-CS** intratumoral injection, no **PS2** fluorescence was detected in the tumor, likely indicating that the **PS2** signal was quenched in the hydrogel network. However, **PS2** associated fluorescence was gradually increasing with time, reaching its peak at 24 h post injection. Of note, **PS2** fluorescence was detected at least until 3 days post-injection. This sustained release is likely mediated by the cleavage of the cross-link bonds at the acidic tumor microenvironment.[54] In contrast, for the **PS2-PBS** solution, **PS2**-associated fluorescence was recorded immediately after injection, but no signal was detected after 24 h. This indicates that free **PS2** is cleared from the tumor within 24 h. The same pattern of **PS2** release was observed for the two tumor models in evaluation. However, the differences between **PS2-PEG-CS** and **PS2-PBS** were significantly higher for CT26 tumors in comparison to those for B16F10 tumors (Figure 6C,D). The different release kinetics,

https://doi.org/10.1021/acs.biomac.3c00591
Biomacromolecules 2024, 25, 24−42

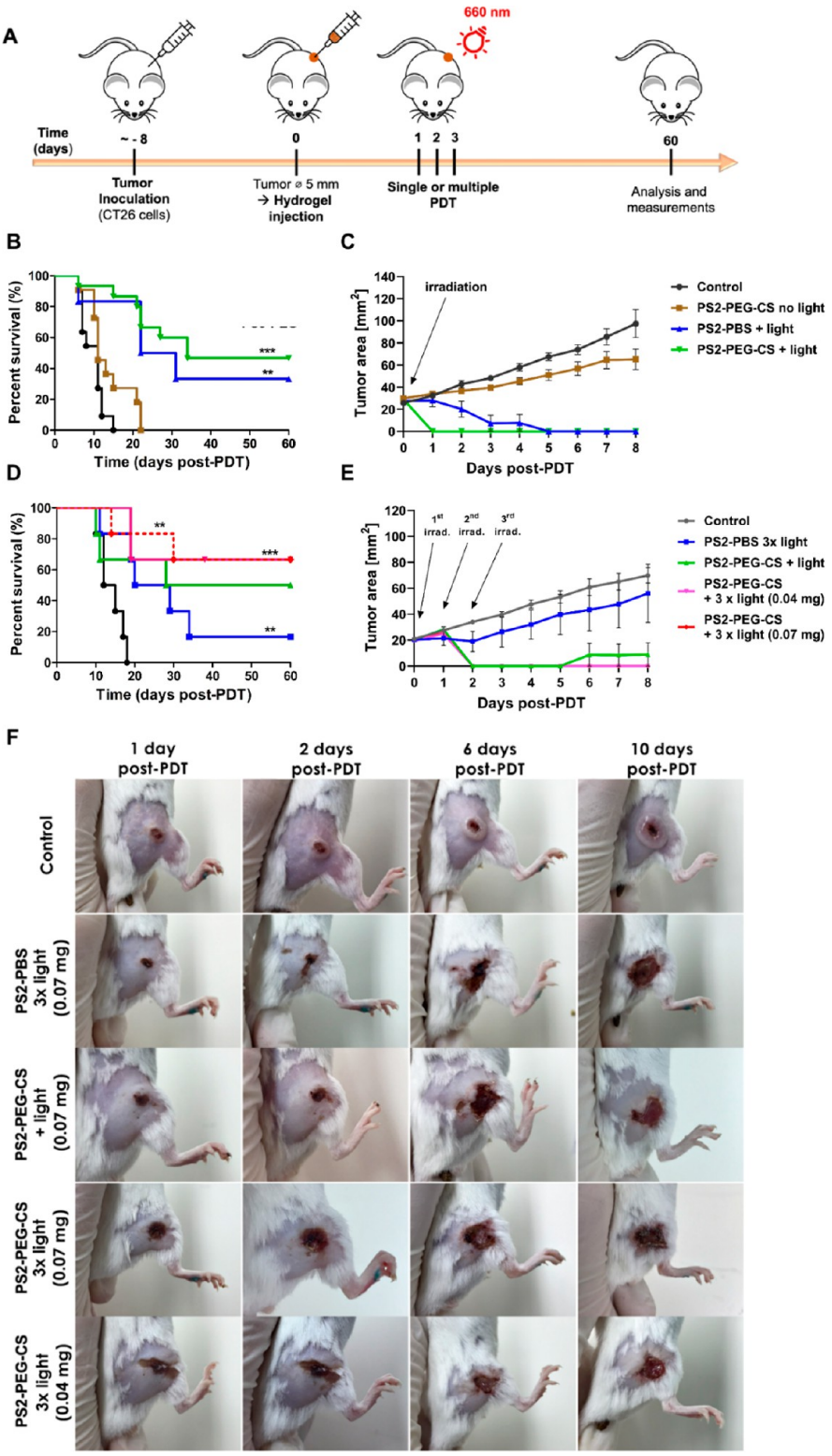

Figure 7. PDT after local administration of **PS2** for the treatment of colon cancer. (A) Schematic illustration of the tumor treatment process against CT26 tumors. (B) Kaplan−Meier survival analysis of male Balb/c mice bearing CT26 tumors treated with the single irradiation PDT protocol using the **PS2-PEG-CS** or **PS2-PBS** formulations. Each treatment group contains 6−15 mice (DLI = 24 h, drug dose 0.07 mg, LD = 20 J/cm^2, and λ = 660 nm); ***$p < 0.001$, **$p < 0.01$ *vs* control. (C) Tumor volume represented as mean ± SEM 8 days post-PDT. (D) Kaplan−Meier survival analysis mice comparing the single and multiple irradiation PDT protocol using the **PS2-PEG-CS** or **PS2-PBS** formulations. Each treatment group contains six mice (DLI = 24, 48, and 72 h, drug dose = 0.04 or 0.07 mg, LD = 20 J/cm^2, and λ = 660 nm). ***$p < 0.001$, **$p < 0.01$ *vs* control. (E) Tumor volume represented as mean ± SEM 8 days post-PDT. (F) Representative images of Balb/c mice treated with single and multiple irradiation PDT protocols using the **PS2-PEG-CS** or **PS2-PBS** formulations.

https://doi.org/10.1021/acs.biomac.3c00591
Biomacromolecules 2024, 25, 24−42

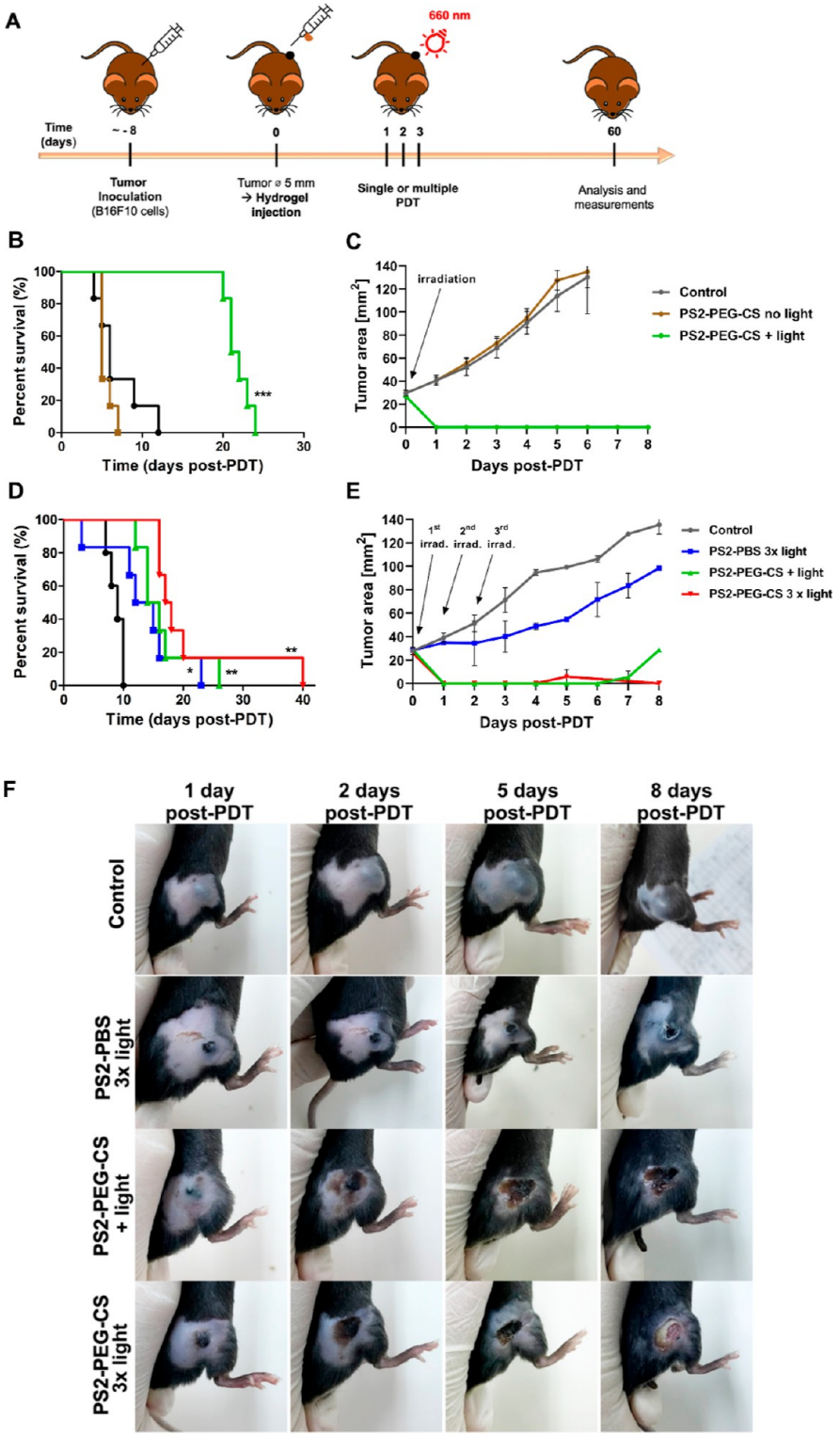

Figure 8. PDT after local administration of **PS2** for the treatment of melanoma tumors. (A) Schematic illustration of the tumor treatment process against B16F10 tumors. (B) Kaplan−Meier survival of female C57BL/6J mice bearing B16F10 tumors after the single irradiation PDT protocol using the **PS2-PEG-CS** hydrogel. Each treatment group consists of six mice (DLI = 24 h, drug dose = 0.08 mg, LD = 36 J/cm^2, and λ = 660 nm). ***p < 0.001 *vs* control. (C) Tumor volume represented as mean ± SEM 8 days post-PDT. (D) Kaplan−Meier survival comparing the single and multiple irradiation PDT protocols using the **PS2-PEG-CS** or **PS2-PBS** formulations. Each treatment group contains six mice (DLI = 24, 48, and 72 h, drug dose = 0.1, LD = 40 J/cm^2, and λ = 660 nm). **p < 0.01, *p < 0.05 *vs* control. (E) Tumor volume represented as mean ± SEM 8 days post-PDT. (F) Representative images of C57BL/6J mice treated with single and multiple irradiation PDT protocols using the **PS2-PEG-CS** or **PS2-PBS** formulations.

and/or clearance rates, in the two tumor models might be related with variances in their tumor microenvironment, specifically in the pH and/or in the tumor blood and lymphatic vasculature.[55,56] On the seventh day, *ex vivo* analysis of the main

https://doi.org/10.1021/acs.biomac.3c00591
Biomacromolecules 2024, 25, 24−42

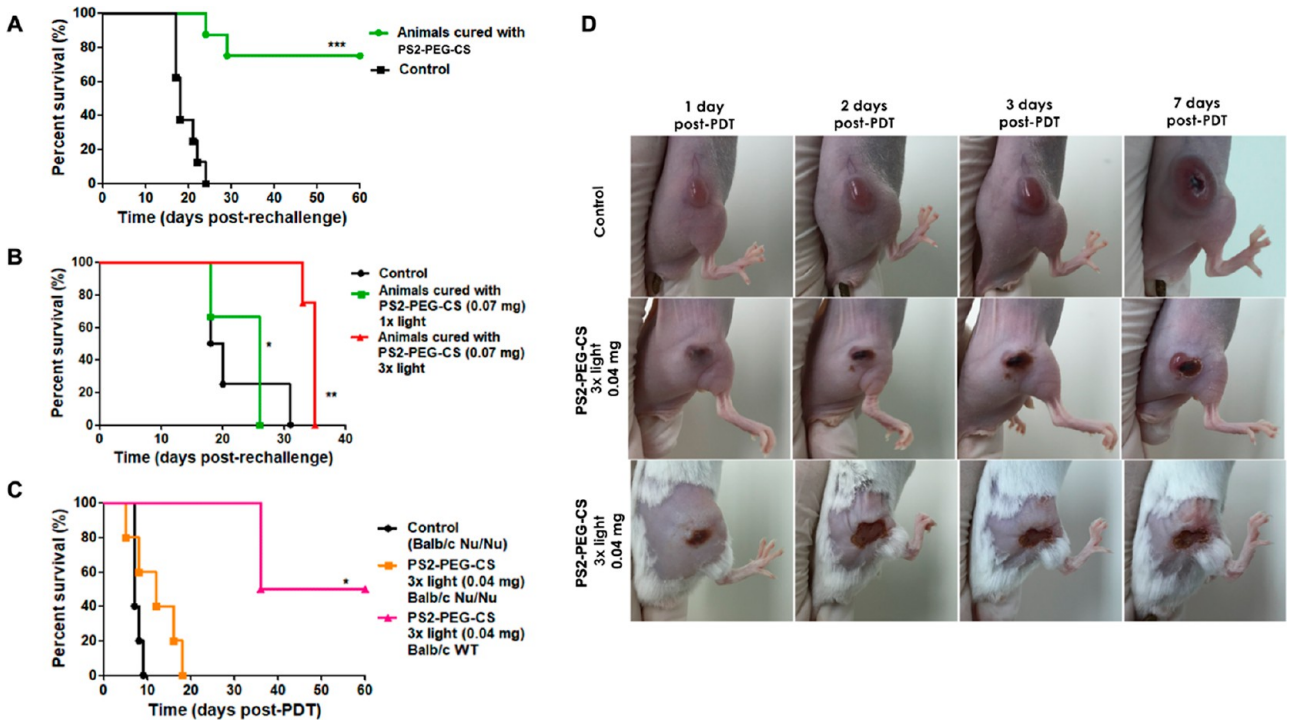

Figure 9. PDT with local administration of **PS2-PEG**-CS induces systemic antitumor immunity. (A) Tumor protection observed following tumor rechallenge (with CT26 cells) of male BALB/c mice that remained CT26 tumor-free for 60 days after PDT using the **PS2-PEG-CS** hydrogel (drug dose = 0.07 mg, DLI = 24 h, LD = 20 J/cm^2). ***$p < 0.001$ *vs* control. (B) Cross-tumor protection observed following tumor rechallenge (with 4T1 cells) of male BALB/c mice that were previously cured, from CT26 tumors, with single or multiple PDT using the **PS2-PEG-CS** hydrogel (drug dose = 0.07 mg, DLI = 24 or 24, 48, and 72 h, LD = 20 J/cm^2); **$p < 0.01$ **PS2-PEG-CS** 3× light *vs* control, *$p < 0.05$ **PS2-PEG-CS** 3× light *vs* **PS2-PEG-CS** 1× light. (C) Survival curves of male Balb/c *vs* male Balb/c nude mice bearing CT26 tumors after treatment with the multiple irradiation PDT protocol using the **PS2-PEG-CS** formulation (DLI = 24, 48, and 72 h, drug dose = 0.04 mg, LD = 20 J/cm^2, and λ = 660 nm). Each treatment group contains five mice. *$p < 0.05$ *vs* control and *vs* **PS2-PEG-CS** 3× light Nu/Nu. (D) Post-PDT images of nude Balb/c and WT Balb/c mice undergoing the multiple irradiation protocol using the **PS2-PEG-CS** formulation (DLI = 24, 48, and 72 h, drug dose = 0.04 mg, LD = 20 J/cm^2, and λ = 660 nm).

organs (bladder, tumor, spleen, liver, muscle, and kidneys) did not reveal any signs of the **PS2** compound (Figure S11). This indicates that **PS2** completely avoids the circulatory system, which might contribute to significantly reduce PDT-associated side effects, like skin photosensitivity.

PDT Using PS2-PEG-CS Hydrogels for the Treatment of CT26 Tumors. An initial optimization was carried out with the **PS2-PEG-CS** hydrogel to select the best PDT conditions. Based on preliminary screenings conducted with a DLI = 24 h, 0.07 mg **PS2**/mouse, with a light dose of 20 J/cm^2, were selected to treat Balb/c mice bearing *sc.* CT26 tumors with an average diameter of 5 mm (Figures S12 and S13). These conditions were then applied to **PS2-PEG-CS** hydrogel and to free **PS2**, which were administered intratumorally using similar volumes (Figure 7A). Strong edema at the irradiated area was observed, both with **PS2-PEG-CS** and **PS2-PBS**, within the first 2 days after illumination. This was followed by progressive necrosis and eschar formation 1 week later. PDT with both the **PS2-PEG-CS** hydrogel and **PS2-PBS** significantly increased the survival rate when compared to the control group (maximum survival of 14 days). 2 months after illumination, tumor-free mice corresponded to 47 and 33%, respectively, for **PS2-PEG-CS** and free **PS2**. No changes relative to the control group were observed with the nonactivated **PS2-PEG-CS**, which indicated a lack of toxicity in the absence of light (Figures 7B,C and S16).

Considering the sustained release of **PS2** at the tumor sites, further improvements were attempted by performing multiple rounds of irradiation. Three tumor irradiations, performed 24, 48, and 72 h after the intratumoral administration of **PS2-PEG-CS** (0.07 mg/mouse), had enabled an increase in the survival rate to 67%, whereas the single illumination protocol had a survival rate of only 50% (Figures 7D,E and S17). Similar results were obtained even when the **PS2** dose was reduced to 0.04 mg/mouse. This shows that the multiple irradiation protocol delivers a better therapeutic response at reduced doses, which might help reduce the likelihood of side effects. In addition, injection of smaller volumes is expected to cause less pain to the patients. It should be noted that the multiple irradiation protocol is more efficient when **PS2** is delivered in the hydrogel formulation than that in its free form (67 *vs* 20% of overall survival) (Figures 7C,D and S14). Images of Balb/c mice treated with single and multiple irradiation PDT protocols using the **PS2-PEG-CS** or **PS2-PBS** formulations are shown in Figures 7F and S14.

PDT Using PS2-PEG-CS Hydrogels for the Treatment of B16F10 Tumors. Next, PDT with **PS2-PEG-CS** was tested in a more challenging tumor model, B16F10 melanoma. Previous studies showed that CT26 tumors respond better to PDT than the B16F10 melanoma tumor model.[57] Several reasons account for the higher aggressiveness of B16F10 melanoma cells. Melanoma is a type of skin cancer characterized by high pigmentation due to the increased melanin production. Melanin absorbs light in UV and visible regions meaning that it can negatively impact the PDT performance.[58] Hyperactivity of melanocyte-based enzymes can cause posttranslational modifications, resulting in inhibition of apoptogenic signaling and leading to resistance to the targeted therapies.[59] Lastly, B16F10

https://doi.org/10.1021/acs.biomac.3c00591
Biomacromolecules 2024, 25, 24−42

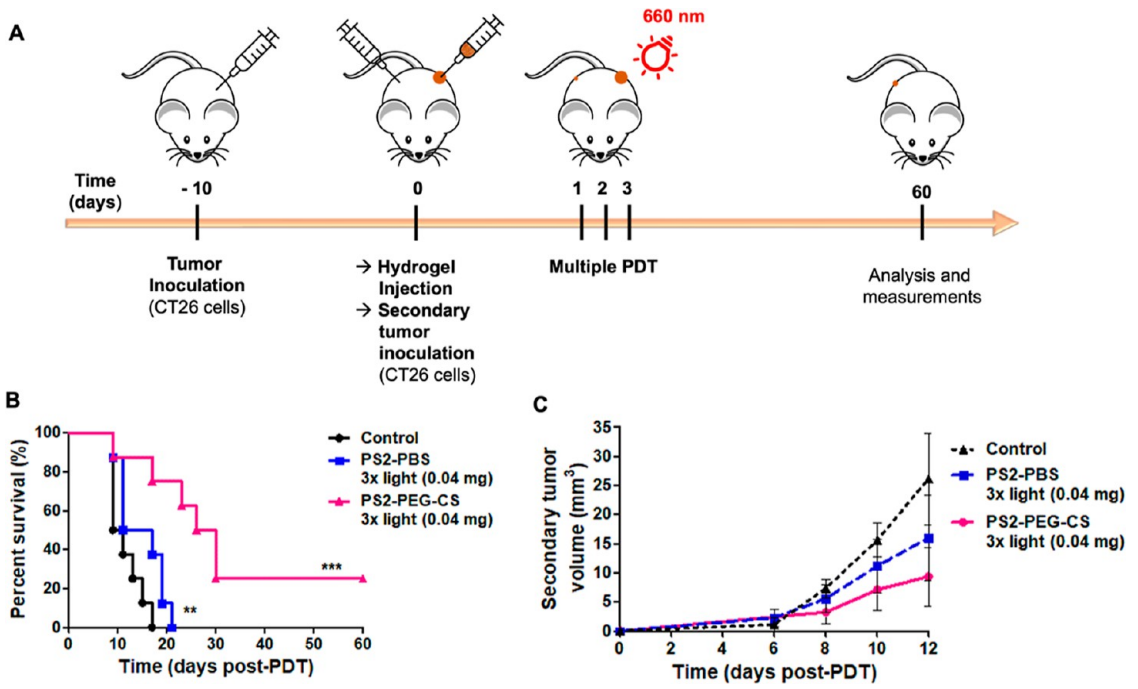

Figure 10. Abscopal effects of PDT with **PS2-PEG-CS** and **PS2-PBS** against distant metastasis. (A) Schematic representation of the experiment of the abscopal effects of PDT with **PS2-PEG-CS** against distant metastasis. (B) Kaplan−Meier survival analysis of male Balb/c mice bearing one CT26 tumor in each flank. The primary tumor was submitted to the PDT multiple irradiation protocol for using the **PS2-PEG-CS** or **PS2-PBS** formulations (DLI = 24, 48, and 72 h, drug dose = 0.07 mg, LD = 20 J/cm^2, and λ = 660 nm). Each treatment group contains eight mice ***$p < 0.001$ *vs* control and **$p < 0.01$ *vs* **PS2-PBS** 3× light. (C) Growth kinetics of secondary tumors which were measured during the time interval where no mouse reached the humane end point. Each treatment group contains eight mice (DLI = 24, 48, and 72 h, drug dose = 0.07 mg, LD = 20 J/cm^2, and λ = 660 nm).

tumors are poorly immunogenic. It was shown in a comprehensive immune profiling study of eight murine solid tumors (CT26, B16F10, 4T1, MAD109, LLC, and RENCA) that the CT26 colon tumor model exhibited high immunogenic profile, while the B16F10 melanoma model was the least immunogenic.[60]

Our first attempt to select the best condition to treat B16F10 tumors included varied **PS2** doses (0.03−0.08 mg) and LDs (20−36 J/cm^2) which were used with a DLI = 24 h (Figure S15). Tumor damage was only observed with the strongest treatment conditions (0.08 mg **PS2**/mouse and DL = 36 J/cm^2), which were then selected for further evaluation (Figure 8A). Mice treated with PDT using **PS2-PEG-CS** exhibited strong inflammation and edema in the irradiated area. Necrosis was visible 2 days post-treatment followed by eschar formation at the end of the first week. For the first 2 weeks post-treatment, there were no signs of tumor growth, and the post-therapeutic wound gradually healed. Although tumor regrowth was observed ∼3 weeks post-PDT, the overall survival time (24 days) was significantly higher when compared with that of the control group (12 days) (Figures 8B,C and S18). No signs of necrosis were observed for inactivated **PS2-PEG-CS**. PDT with **PS1-PEG-CS** was also tested in mice bearing B16F10 tumors, revealing that the administration of 0.06 mg/kg of **PS1-PEG-CS**, combined with a LD of 30 J/cm^2, did not mediate any anticancer effects (Figure S15). This finding aligns with the absence of phototoxicity observed in our *in vitro* studies (Figures 3 and 4).

For the multi-irradiation protocol, 0.1 mg **PS2**/mouse was intratumorally injected followed by three irradiations (40 J/cm^2) at 24, 48, and 72 h postinjection. Mice treated with **PS2-PEG-CS** followed by three irradiations showed the strongest anticancer effects with a median survival rate of 17.5 days, compared to 9 days on the control group. However, comparison between the multi- and the single illumination protocols was revealed to not be statically significant (P value = 0.2158). The multi-irradiation protocol carried out after the administration of the **PS2-PBS** also showed positive outcomes but to a lesser extent than the hydrogel counterparts. For this group, the average post-PDT survival was 13.5 days. Despite the improved therapeutic outcome obtained with the multiple irradiation protocol when **PS2-PEG-CS** was used (median survival of 17.5 days), no permanent tumor remission was attained (Figures 8D,E and S19). Images of C57BL/6J mice treated with single and multiple irradiation PDT protocols using the **PS2-PEG-CS** or **PS2-PBS** formulations are shown in Figure 8F.

PDT with PS2-PEG-CS Induce Antitumor Immunity. PDT is being acknowledged as an import strategy to trigger antitumor immunity.[2,61,62] The inflammation observed after PDT is typically an indicator of the involvement of the immune system. To assess if PDT with the local delivery of **PS2-PEG-CS** activated antitumor immunity with immunological memory, Balb/c mice cured by applying the single irradiation protocol were rechallenged with CT26 cells 60 days post-PDT treatment. Total tumor rejection was observed for 75% of the mice, while all naive animals (control group) exhibited continuous tumor growth (Figure 9A). These results show that **PS2-PEG-CS**-based PDT can induce an antigen-specific immune response capable of stimulating immune memory. The latter enables mice to reject a tumor rechallenge with the same tumor model from which they were cured.

Cross-protection against cells of different origins is rarely reported and often refers to vascular-PDT protocols.[63,64] Balb/c mice cured from CT26 tumors were exposed to 4T1 cells 60

https://doi.org/10.1021/acs.biomac.3c00591
Biomacromolecules 2024, 25, 24−42

days post-PDT. Our results demonstrated that neither the Balb/c mice cured with the single irradiation protocol (0.07 mg of **PS2** and 20 J/cm^2) nor the mice treated with the multiple irradiation protocols (0.07 mg of **PS2** and 3 × 20 J/cm^2), could totally reject the 4T1 cells. However, significantly slowed tumor growth was observed for those mice submitted to the multiple irradiation protocol (35 days) when compared to the single irradiation protocol (26 days) (Figure 9B). The differences on the protection conferred by the single and the multiple irradiation protocols, against 4T1 cells, were statistically significant (P value = 0.014) and may indicate that multiple light stimulations enhanced antitumor immunity. Altogether, these data indicate that PDT with **PS2-PEG-CS** is very effective at stimulating the host immune system.

Immunological memory requires the activation of the adaptive part of the immune system which is typically mediated by T cells.[65,66] To test this hypothesis, the optimized multiple administration protocol was tested in Balb/c nude mice. Balb/c nude mice lack the thymus, which is one of the main organs of the lymphatic system responsible for the production of T lymphocytes.[67] The hydrogel formulation (0.04 mg **PS2**/mouse) was injected intratumorally and was followed by three light irradiations (20 J/cm^2), as previously described. The survival rate dropped from 67 to 0% when WT Balb/c mice were replaced with immunocompromised mice (Figure 9C). Moreover, smaller edema, eschar, and necrotic area were observed in the nude mice (Figure 9D). The differences listed between normal and nude mice demonstrated the importance of an intact immune system, including the presence of T cells, for the long-term effect of PDT with local administration of **PS2-PEG-CS**.

Abscopal Effects of PDT with PS2-PEG-CS against Distant Metastasis. The antitumor immunity elicited by PDT helps control surviving cells at the irradiation site. Additionally, a few studies demonstrated that activation of the host immune system by PDT can inhibit the growth of distant, and non-illuminated, metastases.[65,68−70] To evaluate the abscopal effects of PDT with the local administration of **PS2-PEG-CS**, a double-tumor model was established by inoculating CT26 cells subcutaneously in each flank of the animal with an interval of 10 days (Figure 10A). During the second inoculation, **PS2-PEG-CS** was administered intratumorally into the primary tumor. This was followed by the multiple irradiation protocol, as previously described. The obtained results demonstrated that local PDT not only eradicated the primary tumor (PDT-treated) but also delayed the growth of the untreated contra-lateral tumor (Figure 10B,C). These abscopal effects are a clear sign of systemic antitumor immunity.

Complete inhibition of secondary tumor growth was attained in three out of eight animals when **PS2-PEG-CS** or **PS2-PBS** was used. One mouse in the control group also rejects the secondary inoculation, which can be explained by the first contact with CT26 cells 10 days earlier. Although PDT with **PS2-PEG-CS** and **PS2-PBS** had a similar impact on the untreated and contra-lateral tumors, the overall median survival was more prolonged in the **PS2-PEG-CS** group (28 days) than that in the **PS2-PBS** (14 days) or control (10 days) groups (Figure 10B). The survival of the mice receiving PDT with **PS2-PBS** and of the control group remain below 20 days, whereas mice treated with **PS2-PEG-CS** had extended survival time (two animals with the survival of >60 days).

Discussion. PDT is a highly effective local treatment for cancer that not only elicits a localized response but also triggers robust antitumor immune responses. This phenomenon has been consistently observed and extensively documented by numerous research groups, using a wide range of PSs, namely, porfimer sodium, temoporfin, verteporfin, padeliporfin, redaporfin, chlorin e6, hypericin and 5-ALA.[2,62] While the majority of these studies were conducted using mouse models of cancer, there are also an increasing number of studies demonstrating the induction of antitumor immunity, including the abscopal control of metastasis outside the field of illumination, in cancer patients treated with PDT.[71−77]

The mechanism underlying the immunomodulatory properties of PDT (as well as of other local anticancer therapies) is linked to a specific type of cell death known as immunogenic cell death (ICD).[78] The precise mechanisms behind the ICD are not yet fully understood. However, the enhanced immunogenicity of cancer cells undergoing ICD is attributed to the release and/or exposure of damaged-associated molecular patterns (DAMPs) and tumor-specific antigens in a temporal and spatial manner.[79] For instance, CT26 cells treated with ***m*-THPC** elicit the expression of DAMPs, namely, the surface exposure of calreticulin and release of HMGβ1 and heat shock proteins in CT26 cells. Korbelik *et al.* also showed that the peritumoral administration of CALR immediately after PDT with ***m*-THPC** significantly improved the tumor response, from slightly curative to 40% of cures, in SCCVII tumor-bearing immunocompetent mice but not in immunodeficient NOD/SCID mice.[80]

DAMPs released during ICD further attracted immune cells into the tumor microenvironment. In fact, multiple studies have demonstrated that PDT induces a rapid increase in the number of neutrophils in the blood, which then infiltrate into the tumor mass. Neutrophils and dendritic cells engulf tumor-associated antigens released by dying tumor cells and migrate to the lymph nodes.[5,6,81−87] In the lymph nodes, they prime naive T cells, leading to activation of CD8$^+$ T cells. The latter are then released into the bloodstream and are capable of recognizing remaining tumor cells, both at the primary (and illuminated) tumor and distant metastasis. For this reason, T-cell infiltrates are often observed at tumor sites at later time points after tumor irradiation.[77]

Overall, our *in vivo* data demonstrate the engagement of the immune system following PDT using local administration of **PS2-PEG-CS**. Specifically, it is shown that

(i) 75% of cured mice exhibited tumor rejection when rechallenged with live cancer cells, indicating the presence of adaptive immunity with immunological memory;

(ii) nude mice, which lack T cells, did not achieve any cures, while WT Balb/c mice achieved a 67% cure rate. This observation suggests the involvement of T cells in the PDT outcome using **PS2-PEG-CS**;

(iii) We also observed control of a second tumor lesion located outside the irradiation area, further indicating the presence of systemic antitumor immunity.

The observed antitumor immunity strongly indicates that PDT using **PS2-CS**-based hydrogel effectively eliminates cells in an immunogenic manner. Considering that **PS2** is not efficiently internalized and mainly induces cancer cell death by accidental necrosis, it is suggested that a mechanism similar to that of the Cetuximab-IR700 conjugate is taking place. This conjugate accumulates on the cell surface and, after photoactivation, leads to a necrotic disruption of the plasma membrane. This is followed by the release of pro-inflammatory and immunogenic mediators which trigger strong antitumor immune responses with abscopal effects.[61,88]

https://doi.org/10.1021/acs.biomac.3c00591
Biomacromolecules 2024, 25, 24−42

Other CS-based hydrogels have been previously developed for anticancer PDT, alone[89] or in combination with other therapies,[90] bringing satisfactory results in overcoming PS limitations. However, our work provides the first ***m*-THPC**-loaded hydrogel formulation tested at the preclinical level. The formulation developed, **PS2-PEG-CS**, permits sustained release of the PS, allowing for multi-PDT sessions while also triggering anticancer responses. PDT protocols involving multi-illumination procedures have attracted increased attention in recent years.[15,91] For instance, chlorin e_6 (Ce_6)-loaded peptide-based hydrogels have been proposed for the treatment of MCF-7 tumors. This formulation enabled a sustained release of Ce6 for 48 h with low amounts of the PS being detected even 8 days postinjection. In contrast, free Ce_6 was totally clear from the tumor after 48 h. PDT with six rounds of irradiation at 635 nm (100 mW/cm^2 for 10 min) resulted in a significant delay of tumor growth, but tumor recurrence was appearing after 13 days post-treatment.[91] In another example, a hydrogel composed of poloxamer 407 and poloxamer 188, containing Ce6, was demonstrated to allow controlled release of Ce6 over a period of 7 days. Treatment of mice bearing 4T1 tumors involved two cycles, where each cycle included an intratumoral injection of the hydrogel (0.1 mg/mouse) followed by 3 days of consecutive irradiation. The two cycles were conducted with a 14-day interval between them. The Ce6 hydrogel effectively suppressed the growth of primary tumors and significantly reduced the occurrence of metastasis in the lungs. This effect was attributed to an increase in the infiltration of $CD8^+$ T cells to the tumor microenvironment in samples collected at the end of the study. More recently, an injectable hydrogel containing Prussian blue nanoparticles and CQu (an AIEgen agent) was shown to persist in the tumors for at least 48 h. Inhibition of subcutaneous 4T1 tumors was attained, but this required three cycles of treatment. Each cycle consisted in three rounds of 808 nm laser irradiation (0.5 W/cm^2 during 3 min) that were performed at 0, 24, and 48 h postinjection.[15] Our hydrogel formulation serves the same purpose of achieving "one injection, multiple treatment" but with a reduced number of required irradiations. The results from both tumor models demonstrated that the multiple irradiation protocols resulted in a superior therapeutic response, although some mice still experienced tumor regrowth. The mild cumulative effect observed with multiple irradiations (when compared with the single irradiation protocol) can be attributed to the destruction of the tumor vessels during the first tumor irradiation. Subsequently, this destruction compromises tumor oxygenation, thereby impacting the efficacy of subsequent tumor irradiations.

To address tumor hypoxia and enhance the host immune system, hydrogels can be further formulated with strategies aimed at improving tumor oxygenation and/or immunotherapy. As an example, a recent study reported the development of a sophisticated hydrogel system based on poly(ethylene glycol) double acrylate. This hydrogel formulation contained: (i) the PS Ce6, (ii) catalase, which triggers the rapid decomposition of H_2O_2 into O_2 and, and (iii) imiquimod (R837)-loaded poly(lactic-*co*-glycolic acid) nanoparticles as an immune adjuvant. Designed for the intratumoral injection, this hydrogel system underwent gelation upon light activation, allowing for sustained release of Ce6 and enabling multiple rounds of tumor irradiation. This light-triggered in situ gelation system effectively destroyed tumors and enhanced immune responses after repeated light-triggered PDT sessions. Furthermore, significant improvements were achieved by the combination of the multifunctional hydrogel with an antibody against the anti-cytotoxic T-lymphocyte antigen-4 (α-CTLA4) checkpoint blockade. This combination inhibited the growth of secondary CT26 tumors and led to the increased infiltration of $CD8^+$ T infiltrates. Although promising, this hydrogel system described above exhibits a high level of complexity, which is expected to challenge its clinical translation.[92] In contrast, our approach relies on a simpler hydrogel formulation that not only improves the tolerability of ***m*-THPC** but also delivers good therapeutic outcomes that are linked to immunological memory, without the need for additional immunoadjuvants.

CONCLUSIONS

In summary, we reported the development of a CS-based hydrogel (herein named **PS2-PEG-CS**) for intratumoral injection and controlled release of the ***m*-THPC** derivative, **PS2**. The **PS2-PEG-CS** formulation was characterized by high **PS2** loading and excellent rheological properties that enabled its passage from narrow needles, followed by its reorganization into a 3D hydrogel structure. These features permit the formation of a **PS2** depot at the site of injection enabling a sustained release of the PS drug, which is likely mediated by the acidic cleavage of **PS2-CS** bonds. Importantly, this hydrogel remains for at least 72 h *in vivo* within the tumors, showing that after a single injection, multiple sessions of irradiations were possible. Notably, this strategy accommodates both antitumor and immune-stimulating properties which confer long-lasting memory and control of distant metastasis. The observed antitumor immunity is plausibly linked with the necrotic cell death triggered by the photoactivated **PS2** at the vicinity of the cancer cells. However, the mechanisms underlying ICD in the context of PDT are still poorly understood and deserve further investigation. In the future, we aspire to improve this hydrogel platform by incorporating in its formulation immunoadjuvants (*e.g.*, immune checkpoint blockers) that can boost immunosurveillance.

ASSOCIATED CONTENT

Supporting Information

The Supporting Information is available free of charge at https://pubs.acs.org/doi/10.1021/acs.biomac.3c00591.

Rheological characterization of hydrogels; images of fluorescence microscopy of B16F10 melanoma cells after PDT treatment with **PS2** or ***m*-THPC** activated extracellularly; impact of pharmacological inhibitors of different modalities of cell death on the viability of B16F10 melanoma cells after PDT treatment; histogram of the fluorescence intensities of the oxidized form of the BODIPY 581/591 C11; SEM and TEM of freeze-dried **PS2-PEG-CS**; representative ultrasound images of intratumoral injection of **PS2-PEG-CS** and **PS2-PBS**; ex vivo fluorescence images of the organs collected from C57BL/6J mice 7 days after PDT; and additional Kaplan−Meier survival analysis and graphs representing tumor volume during and post-PDT treatment (PDF)

AUTHOR INFORMATION

Corresponding Authors

Lígia C. Gomes-da-Silva − *CQC, Coimbra Chemistry Center, University of Coimbra, Rua Larga 3004-535 Coimbra, Portugal;* orcid.org/0000-0003-0624-8819; Email: sengem@tcd.ie

https://doi.org/10.1021/acs.biomac.3c00591
Biomacromolecules 2024, 25, 24−42

Mathias O. Senge − *Medicinal Chemistry, Trinity St. James's Cancer Institute, Trinity Translational Medicine Institute, St. James's Hospital, Trinity College Dublin, The University of Dublin, Dublin 8, Ireland; School of Chemistry, Chair of Organic Chemistry, Trinity Biomedical Sciences Institute, Trinity College Dublin, Dublin 2 D02R590, Ireland*; Email: ligia.silva@uc.pt

Authors

Piotr Gierlich − *Medicinal Chemistry, Trinity St. James's Cancer Institute, Trinity Translational Medicine Institute, St. James's Hospital, Trinity College Dublin, The University of Dublin, Dublin 8, Ireland; CQC, Coimbra Chemistry Center, University of Coimbra, Rua Larga 3004-535 Coimbra, Portugal*

Claire Donohoe − *Medicinal Chemistry, Trinity St. James's Cancer Institute, Trinity Translational Medicine Institute, St. James's Hospital, Trinity College Dublin, The University of Dublin, Dublin 8, Ireland; CQC, Coimbra Chemistry Center, University of Coimbra, Rua Larga 3004-535 Coimbra, Portugal*; orcid.org/0000-0003-2468-9431

Kevin Behan − *Trinity Centre for Biomedical Engineering, Trinity Biomedical Sciences Institute, Trinity College Dublin, Dublin 2 D02R590, Ireland*

Daniel J. Kelly − *Trinity Centre for Biomedical Engineering, Trinity Biomedical Sciences Institute, Trinity College Dublin, Dublin 2 D02R590, Ireland*; orcid.org/0000-0003-4091-0992

Complete contact information is available at: https://pubs.acs.org/10.1021/acs.biomac.3c00591

Author Contributions

P.G., C.D., and K.B. performed the experimental work. D.J.K., M.O.S., L.C.G.-d.-S. supervised the work. M.O.S. and L.C.G.-d.-S. conceptualized the project. The manuscript was written through contributions of all authors. All authors have given approval to the final version of the manuscript.

Funding

This project has received funding from the European Union's Horizon 2020 research and innovation program under the Marie Skłodowska-Curie grant agreement number 764837 (Polythea—How light can save lives), the Portuguese Foundation for Science and Technology (UIDB/QUI/00313/2020 and EXPL/BIA-CEL/1295/2021), and the Science Foundation Ireland (SFI award 21/FFP-A/9469). This work was also supported by the Higher Education Authority and the Department of Further and Higher Education, Research, Innovation and Science (Ireland).

Notes

The authors declare no competing financial interest.

■ ACKNOWLEDGMENTS

We thank Dr. Luísa Cortes for providing technical assistance with confocal microscopy and Dr. Andrzej Żak for providing technical assistance with SEM/TEM.

■ ABBREVIATIONS

CS, chitosan; DDS, drug delivery system; DLI, drug-light interval; Em., emission; Ex., excitation; FDA, Food and Drug Administration; G', storage modulus; G'', loss modulus; ICD, immunogenic cell death; ***m*-THPC**, 5,10,15,20-tetrakis(*meta*-hydroxyphenyl)chlorin; PBS, phosphate-buffer saline; PDT, photodynamic therapy; PEG, polyethylene glycol; PS, photosensitizer; ROS, reactive oxygen species

■ REFERENCES

(1) Dąbrowski, J. M.; Arnaut, L. G. Photodynamic therapy (PDT) of cancer: from local to systemic treatment. *Photochem. Photobiol. Sci.* **2015**, *14*, 1765−1780.

(2) Donohoe, C.; Senge, M. O.; Arnaut, L. G.; Gomes-da-Silva, L. C. Cell death in photodynamic therapy: From oxidative stress to anti-tumor immunity. *Biochim. Biophys. Acta, Rev. Cancer* **2019**, *1872*, 188308.

(3) Lorenz, K. J.; Maier, H. Squamous cell carcinoma of the head and neck. Photodynamic therapy with Foscan. *HNO* **2008**, *56*, 402−409.

(4) Gollnick, S. O.; Evans, S. S.; Baumann, H.; Owczarczak, B.; Maier, P.; Vaughan, L.; Wang, W. C.; Unger, E.; Henderson, B. W. Role of cytokines in photodynamic therapy-induced local and systemic inflammation. *Br. J. Cancer* **2003**, *88*, 1772−1779.

(5) Cecic, I.; Parkins, C. S.; Korbelik, M. Induction of systemic neutrophil response in mice by photodynamic therapy of solid tumors. *Photochem. Photobiol.* **2001**, *74*, 712−720.

(6) Sun, J.; Cecic, I.; Parkins, C. S.; Korbelik, M. Neutrophils as inflammatory and immune effectors in photodynamic therapy-treated mouse SCCVII tumours. *Photochem. Photobiol. Sci.* **2002**, *1*, 690−695.

(7) Senge, M. O.; Brandt, J. C. Temoporfin (Foscan, 5,10,15,20-Tetra(*m*-hydroxyphenyl)chlorin)—A Second-generation Photosensitizer. *Photochem. Photobiol.* **2011**, *87*, 1240−1296.

(8) Wiehe, A.; Senge, M. O. The Photosensitizer Temoporfin (*m*THPC) - Chemical, Pre-clinical and Clinical Developments in the Last Decade. *Photochem. Photobiol.* **2023**, *99*, 356−419.

(9) Sasnouski, S.; Zorin, V.; Khludeyev, I.; D'Hallewin, M.-A.; Guillemin, F.; Bezdetnaya, L. Investigation of Foscan® interactions with plasma proteins. *Biochim. Biophys. Acta, Gen. Subj.* **2005**, *1725*, 394−402.

(10) Opitz, I.; Krueger, T.; Pan, Y.; Altermatt, H.-J.; Wagnières, G.; Ris, H.-B. Preclinical Comparison of mTHPC and Verteporfin for Intracavitary Photodynamic Therapy of Malignant Pleural Mesothelioma. *Eur. Surg. Res.* **2006**, *38*, 333−339.

(11) Mitra, S.; Maugain, E.; Bolotine, L.; Guillemin, F.; Foster, T. H. Temporally and Spatially Heterogeneous Distribution of mTHPC in a Murine Tumor Observed by Two-color Confocal Fluorescence Imaging and Spectroscopy in a Whole-mount Model. *Photochem. Photobiol.* **2005**, *81*, 1123−1130.

(12) Triesscheijn, M.; Ruevekamp, M.; Out, R.; Van Berkel, T. J. C.; Schellens, J.; Baas, P.; Stewart, F. A. The pharmacokinetic behavior of the photosensitizer meso-tetra-hydroxyphenyl-chlorin in mice and men. *Cancer Chemother. Pharmacol.* **2007**, *60*, 113−122.

(13) Kübler, A.; de Carpentier, J.; Hopper, C.; Leonard, A. G.; Putnam, G. Treatment of squamous cell carcinoma of the lip using Foscan-mediated Photodynamic Therapy. *Int. J. Oral Maxillofac. Surg.* **2001**, *30*, 504−509.

(14) Wolinsky, J. B.; Colson, Y. L.; Grinstaff, M. W. Local Drug Delivery Strategies for Cancer Treatment: Gels, Nanoparticles, Polymeric Films, Rods, and Wafers. *J. Controlled Release* **2012**, *159*, 14−26.

(15) Zhu, D.; Zheng, Z.; Luo, G.; Suo, M.; Li, X.; Duo, Y.; Tang, B. Z. Single injection and multiple treatments: An injectable nanozyme hydrogel as AIEgen reservoir and release controller for efficient tumor therapy. *Nano Today* **2021**, *37*, 101091.

(16) Merino, S.; Martín, C.; Kostarelos, K.; Prato, M.; Vázquez, E. Nanocomposite Hydrogels: 3D Polymer-Nanoparticle Synergies for On-Demand Drug Delivery. *ACS Nano* **2015**, *9*, 4686−4697.

(17) Li, J.; Mooney, D. J. Designing hydrogels for controlled drug delivery. *Nat. Rev. Mater.* **2016**, *1*, 16071−16117.

(18) Khurana, B.; Gierlich, P.; Meindl, A.; Gomes-da-Silva, L. C.; Senge, M. O. Hydrogels: soft matters in photomedicine. *Photochem. Photobiol. Sci.* **2019**, *18*, 2613−2656.

(19) Andrade, F.; Roca-Melendres, M. M.; Durán-Lara, E. F.; Rafael, D.; Schwartz, S. Stimuli-Responsive Hydrogels for Cancer Treatment:

The Role of pH, Light, Ionic Strength and Magnetic Field. *Cancers* **2021**, *13*, 1164.
(20) Zhou, T.-J.; Xing, L.; Fan, Y.-T.; Cui, P.-F.; Jiang, H.-L. Inhibition of breast cancer proliferation and metastasis by strengthening host immunity with a prolonged oxygen-generating phototherapy hydrogel. *J. Controlled Release* **2019**, *309*, 82−93.
(21) Antony, R.; Arun, T.; Manickam, S. T. D. A review on applications of chitosan-based Schiff bases. *Int. J. Biol. Macromol.* **2019**, *129*, 615−633.
(22) Belali, S.; Emandi, G.; Cafolla, A. A.; O'Connell, B.; Haffner, B.; Möbius, M. E.; Karimi, A.; Senge, M. O. Water-soluble, neutral 3,5-diformyl-BODIPY with extended fluorescence lifetime in a self-healable chitosan hydrogel. *Photochem. Photobiol. Sci.* **2017**, *16*, 1700−1708.
(23) Mi, F.-L.; Sung, H.-W.; Shyu, S.-S. Synthesis and characterization of a novel chitosan-based network prepared using naturally occurring crosslinker. *J. Polym. Sci., Part A-1: Polym. Chem.* **2000**, *38*, 2804−2814.
(24) Ravi Kumar, M. N. V. A review of chitin and chitosan applications. *React. Funct. Polym.* **2000**, *46*, 1−27.
(25) Bhattarai, N.; Gunn, J.; Zhang, M. Chitosan-based hydrogels for controlled, localized drug delivery. *Adv. Drug Delivery Rev.* **2010**, *62*, 83−99.
(26) Gierlich, P.; Mucha, S. G.; Robbins, E.; Gomes-da-Silva, L. C.; Matczyszyn, K.; Senge, M. O. One-Photon and Two-Photon Photophysical Properties of Tetrafunctionalized 5,10,15,20-tetrakis-(m-hydroxyphenyl)chlorin (Temoporfin) Derivatives as Potential Two-Photon-Induced Photodynamic Therapy Agents. *ChemPhotoChem* **2022**, *6*, No. e202100249.
(27) Zhang, Y.; Tao, L.; Li, S.; Wei, Y. Synthesis of Multiresponsive and Dynamic Chitosan-Based Hydrogels for Controlled Release of Bioactive Molecules. *Biomacromolecules* **2011**, *12*, 2894−2901.
(28) Schaberle, F. A. Assessment of the actual light dose in photodynamic therapy. *Photodiagn. Photodyn. Ther.* **2018**, *23*, 75−77.
(29) Olde Damink, L. H. H.; Dijkstra, P. J.; van Luyn, M. J. A.; van Wachem, P. B.; Nieuwenhuis, P.; Feijen, J. Cross-linking of dermal sheep collagen using a water-soluble carbodiimide. *Biomaterials* **1996**, *17*, 765−773.
(30) Ray, M.; Pal, K.; Anis, A.; Banthia, A. K. Development and Characterization of Chitosan-Based Polymeric Hydrogel Membranes. *Des. Monomers Polym.* **2010**, *13*, 193−206.
(31) Boskey, A.; Pleshko Camacho, N. FT-IR imaging of native and tissue-engineered bone and cartilage. *Biomaterials* **2007**, *28*, 2465−2478.
(32) Fu, J.; in het Panhuis, M. Hydrogel properties and applications. *J. Mater. Chem. B* **2019**, *7*, 1523−1525.
(33) Sadat Ebrahimi, M. M.; Schönherr, H. Enzyme-Sensing Chitosan Hydrogels. *Langmuir* **2014**, *30*, 7842−7850.
(34) Mäntele, W.; Deniz, E. UV-VIS absorption spectroscopy: Lambert-Beer reloaded. *Spectrochim. Acta, Part A* **2017**, *173*, 965−968.
(35) Bayat, F.; Karimi, A. R. Design of photodynamic chitosan hydrogels bearing phthalocyanine-colistin conjugate as an antibacterial agent. *Int. J. Biol. Macromol.* **2019**, *129*, 927−935.
(36) Belali, S.; Karimi, A. R.; Hadizadeh, M. Cell-specific and pH-sensitive nanostructure hydrogel based on chitosan as a photosensitizer carrier for selective photodynamic therapy. *Int. J. Biol. Macromol.* **2018**, *110*, 437−448.
(37) Rizwan, M.; Yahya, R.; Hassan, A.; Yar, M.; Azzahari, A. D.; Selvanathan, V.; Sonsudin, F.; Abouloula, C. N. pH Sensitive Hydrogels in Drug Delivery: Brief History, Properties, Swelling, and Release Mechanism, Material Selection and Applications. *Polymers* **2017**, *9*, 137.
(38) Boedtkjer, E.; Pedersen, S. F. The Acidic Tumor Microenvironment as a Driver of Cancer. *Annu. Rev. Physiol.* **2020**, *82*, 103−126.
(39) Boyle, R. W.; Dolphin, D. Structure and Biodistribution Relationships of Photodynamic Sensitizers*. *Photochem. Photobiol.* **1996**, *64*, 469−485.
(40) Donohoe, C.; Schaberle, F. A.; Rodrigues, F. M. S.; Gonçalves, N. P. F.; Kingsbury, C. J.; Pereira, M. M.; Senge, M. O.; Gomes-da-Silva, L. C.; Arnaut, L. G. Unraveling the Pivotal Role of Atropisomerism for Cellular Internalization. *J. Am. Chem. Soc.* **2022**, *144*, 15252−15265.
(41) Pedersen, B. W.; Sinks, L. E.; Breitenbach, T.; Schack, N. B.; Vinogradov, S. A.; Ogilby, P. R. Single Cell Responses to Spatially Controlled Photosensitized Production of Extracellular Singlet Oxygen. *Photochem. Photobiol.* **2011**, *87*, 1077−1091.
(42) Pimenta, F. M.; Jensen, R. L.; Holmegaard, L.; Esipova, T. V.; Westberg, M.; Breitenbach, T.; Ogilby, P. R. Singlet-Oxygen-Mediated Cell Death Using Spatially-Localized Two-Photon Excitation of an Extracellular Sensitizer. *J. Phys. Chem. B* **2012**, *116*, 10234−10246.
(43) Huang, Y.; Liu, Y.; Chen, Y.; Song, M.; Huang, M.; Xue, J.; Liu, L.; Li, J. Probing the interactions of phthalocyanine-based photosensitizers with model phospholipid bilayer by molecular dynamics simulations. *J. Porphyrins Phthalocyanines* **2018**, *22*, 764−770.
(44) Marzorati, M.; Bigler, P.; Vermathen, M. Interactions between selected photosensitizers and model membranes: an NMR classification. *Biochim. Biophys. Acta, Biomembr.* **2011**, *1808*, 1661−1672.
(45) Ricchelli, F. Photophysical properties of porphyrins in biological membranes. *J. Photochem. Photobiol., B* **1995**, *29*, 109−118.
(46) White, W. I. *The Porphyrins*; Dolphin, D., Ed.; Academic Press: New York, 2012; Vol. *5*, pp 303−335.
(47) Hestand, N. J.; Spano, F. C. Expanded Theory of H- and J-Molecular Aggregates: The Effects of Vibronic Coupling and Intermolecular Charge Transfer. *Chem. Rev.* **2018**, *118*, 7069−7163.
(48) Nakajima, K.; Ogawa, M. Phototoxicity in near-infrared photoimmunotherapy is influenced by the subcellular localization of antibody-IR700. *Photodiagn. Photodyn. Ther.* **2020**, *31*, 101926.
(49) Darzynkiewicz, Z.; Juan, G.; Li, X.; Gorczyca, W.; Murakami, T.; Traganos, F. Cytometry in cell necrobiology: Analysis of apoptosis and accidental cell death (necrosis). *Cytometry* **1997**, *27*, 1−20.
(50) Stark, G. Functional Consequences of Oxidative Membrane Damage. *J. Membr. Biol.* **2005**, *205*, 1−16.
(51) Ogawa, E.; Ito, A.; Arai, T. Detailed in vitro study of the photosensitization reaction of extracellular talaporfin sodium in rat myocardial cells. *Lasers Surg. Med.* **2013**, *45*, 660−667.
(52) Drummen, G. P. C.; van Liebergen, L. C. M.; Op den Kamp, J. A. F.; Post, J. A. C11-BODIPY581/591, an oxidation-sensitive fluorescent lipid peroxidation probe: (micro)spectroscopic characterization and validation of methodology. *Free Radical Biol. Med.* **2002**, *33*, 473−490.
(53) Girotti, A. W. Photosensitized oxidation of membrane lipids: Reaction pathways, cytotoxic effects, and cytoprotective mechanisms. *J. Photochem. Photobiol., B* **2001**, *63*, 103−113.
(54) Mo, R.; Gu, Z. Tumor microenvironment and intracellular signal-activated nanomaterials for anticancer drug delivery. *Mater. Today* **2016**, *19*, 274−283.
(55) He, Q.; Chen, J.; Yan, J.; Cai, S.; Xiong, H.; Liu, Y.; Peng, D.; Mo, M.; Liu, Z. Tumor microenvironment responsive drug delivery systems. *Asian J. Pharm. Sci.* **2020**, *15*, 416−448.
(56) Webb, S. D.; Sherratt, J. A.; Fish, R. G. Mathematical Modelling of Tumor Acidity: Regulation of Intracellular pH. *J. Theor. Biol.* **1999**, *196*, 237−250.
(57) Pucelik, B.; Arnaut, L. G.; Stochel, G.; Dąbrowski, J. M. Design of Pluronic-Based Formulation for Enhanced Redaporfin-Photodynamic Therapy against Pigmented Melanoma. *ACS Appl. Mater. Interfaces* **2016**, *8*, 22039−22055.
(58) Barun, V. V.; Ivanov, A. P.; Volotovskaya, A. V.; Ulashchik, V. S. Absorption spectra and light penetration depth of normal and pathologically altered human skin. *J. Appl. Spectrosc.* **2007**, *74*, 430−439.
(59) Premi, S. Role of Melanin Chemiexcitation in Melanoma Progression and Drug Resistance. *Front. Oncol.* **2020**, *10*, 1305.
(60) Zhong, W.; Myers, J. S.; Wang, F.; Wang, K.; Lucas, J.; Rosfjord, E.; Lucas, J.; Hooper, A. T.; Yang, S.; Lemon, L. A.; Guffroy, M.; May, C.; Bienkowska, J. R.; Rejto, P. A. Comparison of the molecular and cellular phenotypes of common mouse syngeneic models with human tumors. *BMC Genomics* **2020**, *21*, 2.
(61) Gomes-da-Silva, L. C.; Kepp, O.; Kroemer, G. Regulatory approval of photoimmunotherapy: photodynamic therapy that induces immunogenic cell death. *OncoImmunology* **2020**, *9*, 1841393.
(62) Lobo, C. S.; Gomes-da-Silva, L. C.; Arnaut, L. G. 222: Potentiation of Systemic Anti-Tumor Immunity with Photodynamic

https://doi.org/10.1021/acs.biomac.3c00591
Biomacromolecules 2024, 25, 24−42

Therapy Using Porphyrin Derivatives. In *Handbook of Porphyrin Science*; Kadish, K., Smith, K. M., Guilard, R., Eds.; World Scientific: London, 2022; Vol. *46*, pp 279−344.
(63) Preise, D.; Oren, R.; Glinert, I.; Kalchenko, V.; Jung, S.; Scherz, A.; Salomon, Y. Systemic antitumor protection by vascular-targeted photodynamic therapy involves cellular and humoral immunity. *Cancer Immunol., Immunother.* **2009**, *58*, 71−84.
(64) Zhang, Y.; Cheung, Y.-K.; Ng, D. K. P.; Fong, W.-P. Enhancement of innate and adaptive anti-tumor immunity by serum obtained from vascular photodynamic therapy-cured BALB/c mouse. *Cancer Immunol., Immunother.* **2021**, *70*, 3217−3233.
(65) Rocha, L. B.; Gomes-da-Silva, L. C.; Dąbrowski, J. M.; Arnaut, L. G. Elimination of primary tumours and control of metastasis with rationally designed bacteriochlorin photodynamic therapy regimens. *Eur. J. Cancer* **2015**, *51*, 1822−1830.
(66) Lobo, A. C. S.; Gomes-da-Silva, L. C.; Rodrigues-Santos, P.; Cabrita, A.; Santos-Rosa, M.; Arnaut, L. G. Immune Responses after Vascular Photodynamic Therapy with Redaporfin. *J. Clin. Med.* **2020**, *9*, 104.
(67) Szadvari, I.; Krizanova, O.; Babula, P. Athymic nude mice as an experimental model for cancer treatment. *Physiol. Res.* **2016**, *65*, S441−S453.
(68) Yang, G.; Xu, L.; Xu, J.; Zhang, R.; Song, G.; Chao, Y.; Feng, L.; Han, F.; Dong, Z.; Li, B.; Liu, Z. Smart Nanoreactors for pH-Responsive Tumor Homing, Mitochondria-Targeting, and Enhanced Photodynamic-Immunotherapy of Cancer. *Nano Lett.* **2018**, *18*, 2475−2484.
(69) He, C.; Duan, X.; Guo, N.; Chan, C.; Poon, C.; Weichselbaum, R. R.; Lin, W. Core-shell nanoscale coordination polymers combine chemotherapy and photodynamic therapy to potentiate checkpoint blockade cancer immunotherapy. *Nat. Commun.* **2016**, *7*, 12499.
(70) Kleinovink, J. W.; Fransen, M. F.; Löwik, C. W.; Ossendorp, F. Photodynamic-Immune Checkpoint Therapy Eradicates Local and Distant Tumors by CD8+ T Cells. *Cancer Immunol. Res.* **2017**, *5*, 832−838.
(71) Abdel-Hady, E.-S.; Martin-Hirsch, P.; Duggan-Keen, M.; Stern, P. L.; Moore, J. V.; Corbitt, G.; Kitchener, H. C.; Hampson, I. N. Immunological and Viral Factors Associated with the Response of Vulval Intraepithelial Neoplasia to Photodynamic Therapy1. *Cancer Res.* **2001**, *61*, 192−196.
(72) Kabingu, E.; Oseroff, A. R.; Wilding, G. E.; Gollnick, S. O. Enhanced Systemic Immune Reactivity to a Basal Cell Carcinoma Associated Antigen Following Photodynamic Therapy. *Clin. Cancer Res.* **2009**, *15*, 4460−4466.
(73) Longo, C.; Casari, A.; Pepe, P.; Moscarella, E.; Zalaudek, I.; Argenziano, G.; Pellacani, G. Confocal Microscopy Insights into the Treatment and Cellular Immune Response of Basal Cell Carcinoma to Photodynamic Therapy. *Dermatology* **2012**, *225*, 264−270.
(74) Reginato, E.; Lindenmann, J.; Langner, C.; Schweintzger, N.; Bambach, I.; Smolle-Jüttner, F.; Wolf, P. Photodynamic therapy downregulates the function of regulatory T cells in patients with esophageal squamous cell carcinoma. *Photochem. Photobiol. Sci.* **2014**, *13*, 1281−1289.
(75) Theodoraki, M. N.; Lorenz, K.; Lotfi, R.; Fürst, D.; Tsamadou, C.; Jaekle, S.; Mytilineos, J.; Brunner, C.; Theodorakis, J.; Hoffmann, T. K.; Laban, S.; Schuler, P. J. Influence of photodynamic therapy on peripheral immune cell populations and cytokine concentrations in head and neck cancer. *Photodiagn. Photodyn. Ther.* **2017**, *19*, 194−201.
(76) Thong, P. S.-P.; Ong, K.-W.; Goh, N. S.-G.; Kho, K.-W.; Manivasager, V.; Bhuvaneswari, R.; Olivo, M.; Soo, K.-C. Photodynamic-therapy-activated immune response against distant untreated tumours in recurrent angiosarcoma. *Lancet Oncol.* **2007**, *8*, 950−952.
(77) Gu, B.; Wang, B.; Li, X.; Feng, Z.; Ma, C.; Gao, L.; Yu, Y.; Zhang, J.; Zheng, P.; Wang, Y.; Li, H.; Zhang, T.; Chen, H. Photodynamic therapy improves the clinical efficacy of advanced colorectal cancer and recruits immune cells into the tumor immune microenvironment. *Front. Immunol.* **2022**, *13*, 1050421.
(78) Kepp, O.; Marabelle, A.; Zitvogel, L.; Kroemer, G. Oncolysis without viruses — inducing systemic anticancer immune responses with local therapies. *Nat. Rev. Clin. Oncol.* **2020**, *17*, 49−64.
(79) Kroemer, G.; Galassi, C.; Zitvogel, L.; Galluzzi, L. Immunogenic cell stress and death. *Nat. Immunol.* **2022**, *23*, 487−500.
(80) Korbelik, M.; Banáth, J.; Saw, K. M.; Zhang, W.; Čiplys, E. Calreticulin as Cancer Treatment Adjuvant: Combination with Photodynamic Therapy and Photodynamic Therapy-Generated Vaccines. *Front. Oncol.* **2015**, *5*, 15.
(81) Cecic, I.; Stott, B.; Korbelik, M. Acute phase response-associated systemic neutrophil mobilization in mice bearing tumors treated by photodynamic therapy. *Int. Immunopharmacol.* **2006**, *6*, 1259−1266.
(82) Cecic, I.; Sun, J.; Korbelik, M. Role of complement anaphylatoxin C3a in photodynamic therapy-elicited engagement of host neutrophils and other immune cells. *Photochem. Photobiol.* **2006**, *82*, 558−562.
(83) Cecic, I.; Korbelik, M. Mediators of peripheral blood neutrophilia induced by photodynamic therapy of solid tumors. *Cancer Lett.* **2002**, *183*, 43−51.
(84) Garg, A. D.; Vandenberk, L.; Fang, S.; Fasche, T.; Van Eygen, S.; Maes, J.; Van Woensel, M.; Koks, C.; Vanthillo, N.; Graf, N.; de Witte, P.; Van Gool, S.; Salven, P.; Agostinis, P. Pathogen response-like recruitment and activation of neutrophils by sterile immunogenic dying cells drives neutrophil-mediated residual cell killing. *Cell Death Differ.* **2017**, *24*, 832−843.
(85) Brackett, C. M.; Muhitch, J. B.; Evans, S. S.; Gollnick, S. O. IL-17 Promotes Neutrophil Entry into Tumor-Draining Lymph Nodes following Induction of Sterile Inflammation. *J. Immunol.* **2013**, *191*, 4348−4357.
(86) Kousis, P. C.; Henderson, B. W.; Maier, P. G.; Gollnick, S. O. Photodynamic Therapy Enhancement of Antitumor Immunity Is Regulated by Neutrophils. *Cancer Res.* **2007**, *67*, 10501−10510.
(87) Sasnouski, S.; Zorin, V.; Khludeyev, I.; D'Hallewin, M.-A.; Guillemin, F.; Bezdetnaya, L. Investigation of Foscan® interactions with plasma proteins. *Biochim. Biophys. Acta, Gen. Subj.* **2005**, *1725*, 394−402.
(88) Mączyńska, J.; Da Pieve, C.; Burley, T. A.; Raes, F.; Shah, A.; Saczko, J.; Harrington, K. J.; Kramer-Marek, G. Immunomodulatory activity of IR700-labelled affibody targeting HER2. *Cell Death Dis.* **2020**, *11*, 886.
(89) Xia, L.-Y.; Zhang, X.; Cao, M.; Chen, Z.; Wu, F.-G. Enhanced Fluorescence Emission and Singlet Oxygen Generation of Photosensitizers Embedded in Injectable Hydrogels for Imaging-Guided Photodynamic Cancer Therapy. *Biomacromolecules* **2017**, *18*, 3073−3081.
(90) Zhang, Z.; Li, A.; Min, X.; Zhang, Q.; Yang, J.; Chen, G.; Zou, M.; Sun, W.; Cheng, G. An ROS-sensitive tegafur-PpIX-heterodimer-loaded in situ injectable thermosensitive hydrogel for photodynamic therapy combined with chemotherapy to enhance the tegafur-based treatment of breast cancer. *Biomater. Sci.* **2021**, *9*, 221−237.
(91) Abbas, M.; Xing, R.; Zhang, N.; Zou, Q.; Yan, X. Antitumor Photodynamic Therapy Based on Dipeptide Fibrous Hydrogels with Incorporation of Photosensitive Drugs. *ACS Biomater. Sci. Eng.* **2018**, *4*, 2046−2052.
(92) Meng, Z.; Zhou, X.; Xu, J.; Han, X.; Dong, Z.; Wang, H.; Zhang, Y.; She, J.; Xu, L.; Wang, C.; Liu, Z. Light-Triggered In Situ Gelation to Enable Robust Photodynamic-Immunotherapy by Repeated Stimulations. *Adv. Mater.* **2019**, *31*, 1900927.

https://doi.org/10.1021/acs.biomac.3c00591
Biomacromolecules 2024, 25, 24−42